Electron spin resonance (some chemical applications)

Christopher J. Rhodes
DOI: 10.1039/b417213m

The field of ESR (or EPR) continues apace, predominantly as further applications are discovered for the method. As in all aspects of modern life, some of the greatest advances in the area of ESR and free-radical (paramagnetic) chemistry have arisen through the immense developments made in computing, and so we may witness not only supplements in instrumentation, *e.g.* pulsed ESR and ENDOR/TRIPLE methods, but also in theoretical techniques, most strikingly through the agency of Density Functional Theory (DFT), which, reminded of my early adventures with semi-empirical methods such as INDO, now appear to accurately reproduce experimental hyperfine coupling constants (always a challenging task for ''open-shell'' systems), and the energetics of paramagnetic molecular configurations.

1. Introduction

It is, once again, a pleasure to respond to Professor Webb's invitation to write a review covering the scientific literature on the technique of Electron Spin Resonance (ESR) and its many applications. Two years ago, I wrote a similar article[1] in this series that focused particularly on applications of ESR to the biological and environmental sciences. This time, my emphasis will be mainly on applications in chemistry and the chemical sciences. Though this article covers mainly 2004, the topics presented are, in my opinion, a fair illustration of the current state of play in ESR research. I found that the literature topics tended to sift themselves into the following broad headings, much as they did in my last coverage of ESR-based chemistry in 1999,[2] although there have been many new discoveries made since then. Thus, the papers essentially fall into general aspects of 'organic', 'inorganic', 'theoretical', 'instrumental', 'biology and medicine', and 'materials'. There will be considerable overlap between these areas as, is the truth of contemporary research, and as I wrote in 1999, the aim of my words are to offer ''what ESR can do for *you*, be you a chemist, biochemist, materials, environmental, or any other kind of scientist''. On the matter of ''ESR'', Electron Spin Resonance, or ''EPR'', Electron Paramagnetic Resonance: although the latter is the official term, it is not used by everybody, and so I shall use whichever acronym authors have chosen when referring to particular papers.

2. Technical and theoretical

There are a number of novel instruments and approaches that have been reported during the review period, potentially in relation to biology and medicine; subjects

Fresh-Lands, P.O. Box 2074, Reading, UK RG4 5ZQ. E-mail: cjrhodes@fresh-lands.com

which, along with environmental science (and sometimes psychology, as universities restructure themselves), are often referred to collectively as the "Life Sciences". For example, a spectrometer which offers the possibility of both continuous-wave and pulsed measurements at 275 GHz (wavelength 1.1 mm) has been developed.[3] In order to match this high frequency, a magnetic field of 9.9 T is required, supplied by a superconducting solenoid. The microwave bridge uses partly quasi-optical components, and a cylindrical cavity gives a high filling factor and a high sensitivity. $\pi/2$ pulses down to 100 ns are possible, with a microwave power of 1 mW. At the other end of the frequency scale, an L-band (1–1.5 GHz) resonator has been developed, this time for providing three-dimensional imaging.[4] This is a 3-loop 2-gap re-entrant resonator that can accommodate aqueous samples of up to 20 mm diameter and 30 mm length. Matching between the resonator and the microwave bridge was achieved by a coupling loop inserted into one of the two lateral arms. For the unloaded cavity, the optimum diameter of the coupling loop was found to be about one-third that of the arm diameter, while for the loaded cavity it was almost equal to the cavity arm diameter. The spatial distribution of TEMPO (2,2,6,6-tetramethyl-piperidine-1-oxyl) radicals was determined in a sample tube. Another paper describes the design and performance of an ESR spectrometer that operates using a 9 T superconducting magnet, but at 3 or 9 GHz frequencies.[5] The probe head contains a compact 2-loop, 1-gap resonator that is embedded into the variable temperature insert of the magnet, so enabling measurements to be made at fields between 0 and 9 T and over the temperature range 1.5–400 K. The spectrometer is useful in that it may be employed to investigate systems where resonance occurs at fields far above that for the $g = 2$ condition, such as in strongly coupled spin systems. The low quality factor of the resonator allows time-resolved experiments, for example, longitudinally-detected ESR, to be made. Its performance is demonstrated on the MgB_2 superconductor and the RbC_{60} conducting alkali-fulleride polymer. A non-radiative approach to single-mode dielectric resonators has been developed.[6] It is expected that a dielectric resonator will give a better performance overall, in comparison to a metallic cavity, as is well established at low frequencies. At higher frequencies the situation is more complex, in terms of the properties of the materials employed and other considerations. Successful preliminary measurements made at frequencies close to 90 and 180 GHz are reported, and the particular advantages of the proposed resonator are discussed in comparison with the performance of a conventional cavity. Goldfarb's group have reported on methods for improving the sensitivity of pulsed ENDOR and special TRIPLE at W-band.[7] Two approaches were employed, one of which eliminates baseline problems while the other enhances the ENDOR effect. The baselines, measured using pulsed ENDOR at high fields from samples at low temperatures, are often distorted by the heating effect of the RF pulses which causes some de-tuning of the cavity and consequently leads to a loss of echo intensity. Since this often masks broad and weak ENDOR signals, it is a serious problem. However, it can be eliminated by recording the ENDOR spectra in a random rather than a sequential variation of the RF. The signal to noise of the ENDOR spectrum can be significantly enhanced by the application of the pulse analogue of the continuous wave (CW) special TRIPLE experiment, which is very efficient at W-band frequencies although it would not work at X-band.

A new programme has been developed for the analysis of superhyperfine interactions in CW ESR spectroscopy, and is based on an extension of Freed's analysis of the motion of nitroxide probes in liquids, in order to obtain information on motional dynamics. Since Freed's approach analysed the hyperfine interaction of a single

nucleus, it is difficult to extend it to a copper complex, which has more than one hyperfine interaction. A preliminary version is presented, which does not include a restoring potential, and so can be used only under isotropic conditions.[8] Bales *et al.* report[9] an extension of previous work that allows the simulation of inhomogeneously broadened nitroxide spectra, consisting of five hyperfine lines from the coupling to two equivalent ^{14}N nuclei. The nitronyl-nitroxide 1-*H*-imidazol-1-yloxy-4,5-dihydro-4,4,5,5-tetramethyl-2-(*ortho*-nitrophenyl)-3-oxide is severely inhomogeneously broadened by unresolved hyperfine structure in the absence of spin-exchange, and was studied under conditions where the spin-exchange frequency varies from close to zero to more than half of the hyperfine splitting. In common with their previous paper,[10] the authors find a series of criteria regarding the spectral line intensities for this radical as the exchange frequency increases. The line-shifts are not well reproduced by theory, unless spin-precession during the act of spin-exchange and re-encounters of the same spins during one collision are included. A time between re-encounters of 100 ps is estimated, and is of the correct order of magnitude to that predicted from a Stokes–Einstein diffusion model. It is thought that inclusion of the effect of re-encounters should allow a deeper understanding of the nature of the collision process in terms of liquid structure. A paper[11] has appeared which describes a study of the dynamics of sugar-bound spin probes in sucrose solution at L-, X- and W-band frequencies; specifically, at 0.7, 9.4 and 94 GHz. The linewidths of two glycosidated probes, 4-(α,β-D-glucopyranosyloxy)-TEMPO (Glc-TEMPO) and 4-(α,β-D-lactopyranosyloxy)-TEMPO (Lac-TEMPO), and one non-glycosylated probe, 4-hydroxy-TEMPO (TEMPOL), were investigated in order to determine some fundamental hydrodynamic properties of sugar-bound spin probes. The linewidths were measured in solutions containing between 0–50 wt% of sucrose. The benefit of the multi-frequency approach is that, by its means, a full characterisation of the linewidth parameters is possible, which provides an insight into the overall molecular shape of the probe molecules in the sucrose solutions. An analysis based on the fast-motional linewidth theory yields values which indicate that the glycosidated probes have a prolate-type shape that is elongated along the x-axis (N–O axis), with the elongation being more marked for Lac-TEMPO. The interaction parameters (ratios of the effective hydrodynamic volumes to the actual volumes), corrected for the difference in molecular shape, were found to lie in the order TEMPOL < Glc-TEMPO < Lac-TEMPO, in accordance with the expectation that the glycosidated spin probes will exhibit stronger hydrogen bonding to an aqueous medium. By employing 90° out-of-phase first-harmonic absorption ESR (V'_1-ESR), obtaining the spectra of nitroxide spin labels with differing T_1 relaxation times is possible.[12] Non-linear V'_1-ESR spectra, recorded under conditions of moderate saturation, were found to have lines that are sharper than those recorded using in-phase V'_1-ESR, and have amplitudes that preferentially enhance signals from species with longer T_1 relaxation times. A further discrimination may be achieved in the presence of selective paramagnetic relaxation enhancement agents. Examples are given of biophysical applications to double spin-labelled single-component membranes, lipid–peptide complexes and the binding of spin-labelled reagents.

A review[13] of spin Hamiltonians that are applicable to exchange-coupled systems in relation to biomaterials has appeared. Dinuclear and tetranuclear complexes of spin-coupled Mn–Mn, Mn–Fe and Fe–Fe ions occur in enzymes that are of central relevance in biology, *e.g.* photosynthesis. These complexes contain oxidation states of Mn and Fe that are higher than is normally encountered for the cations of these

elements. Various approaches to the analysis of the ESR spectra of these systems are compared and contrasted. The effects[14] of either static or pulsed magnetic fields on the rate of the reaction between Fremy's salt and ascorbic acid have been investigated, and are accountable within the radical pair mechanism. Since the effects are small, they were enhanced using a field gradient technique, which is reported to detect both the reacting radicals and the radical intermediates involved in the reaction. Freed's group report[15] a method for the measurement of relatively large distances in biomolecules using double-quantum filtered refocused electron spin-echos. This novel technique is a significant improvement over double-quantum coherence ESR because it increases the experimental acquisition times. The method is demonstrated using a long double-strand of A-type RNA that had been spin-labelled at both ends, from which a distance of 72 Å was deduced, in excellent agreement with molecular modelling. A way to improve the sensitivity of pulse EPR distance measurements has been reported.[16] In contrast to established pulse EPR methods, which measure small dipole–dipole couplings between electron spins using constant time echo experiments, this one employs a variable time method. Comparisons between the two modes are made when measuring the end-to-end distances of 5 and 7.5 nm of rod-like, shape-persistent biradicals, and for the measurement of a broadly distributed trans-membrane distance in a doubly spin-labelled mutant of light harvesting PS complex II (PS II = photosystem II). From a study of the hexamethylethane radical cation in liquid hexane, an evaluation was made of the time-resolved magnetic field effect in detecting short-lived radical intermediates.[17] The ESR spectrum of the hexamethylethane radical cation in solution is characterised by an isotropic coupling to eighteen equivalent protons. Both the hyperfine coupling constant and the difference in *g*-values with the *para*-terphenyl-d_{14} radical anion are in agreement with the data determined using the optical detection method. The dependence of reaction rates on the magnetic field strength are derived and possible relaxation mechanisms discussed. The effects[18] of anisotropic motion in non-linear CW EPR spectra have been shown to enhance the relaxation of lipid spin-labels, which allows the determination of the location of spin labels in, *e.g.*, membrane systems. The focus of this paper is the effects of anisotropic diffusion and ordering on non-linear CW ESR methods for determining the T_1 values of spin-labels. Various motional models are considered and some experimental examples are given for spin-labelled lipids in membranes. In another paper,[19] homogeneous linewidths, characterised by the phase-memory time T_m, of a nitroxide spin-labelled peptide were measured over the entire motional range (10^{-10} s to 10^{-4} s) at X-band frequencies using spin-echo correlated spectroscopy (SECSY) ESR. Phase memory times down to 20 ns could be determined by minimising the effects of pulse ring-down. The curve of the experimental T_m *vs.* temperature (from 192 to 310 K) permits the determination of the T_m minimum, and is a sensitive aid in unravelling details of the molecular dynamics.

A review has appeared about the use of EPR power saturation to analyse the membrane-docking geometries of peripheral proteins.[20] It is contended that although peripheral membrane proteins are centrally important in cellular signaling and metabolic pathways, the precise natural the protein–membrane interface is illusive to high-resolution structural methods. However, a number of laboratories have each made their own contributions to the development of an ESR (EPR) power saturation methodology that use site-directed spin-labelling to determine the major geometric parameters of membrane-bound proteins, particularly their penetration depths and angular orientations relative to the membrane surface. A description of

some applications of the approach to Ca^{2+}-activated membrane docking domains is given. The influence of ionising radiation on small molecules—certainly by biological standards—has been studied extensively using ESR, in an overall aim to obtain fundamental information about these far more complex systems. Nonetheless, even the results from such relatively simple models are not always clear-cut in their interpretation. For example, when single crystals are irradiated, the measurement of electronic *g*-factors is frequently very difficult because more than one radical may arise, and the overall EPR pattern is a composite of several components, *e.g.*, from multiple radicals and of multiple radical sites within the crystal. On the other hand, if an ENDOR line can be fully resolved, the method of ENDOR-induced EPR, in principle at least, allows the identification of the EPR spectrum corresponding to that line. The approach was tried on known systems malonic acid and guanine hydrochloride dihydrate, for which good agreement was obtained with the values known from EPR measurements for the radicals $CH^{\bullet}(COOH)_2$ and the O6-protonated guanine radical anion.[21] A kinetic model of the dynamics of photochemical reactions exhibiting chemically-induced electron spin polarisation (CIDEP) is presented, which includes all relevant parameters, including reaction of the excited precursor as both a singlet and a triplet, and spin-exchange during radical encounters. By its means, an analysis of the acetone/propan-2-ol photolytic system reveals spin-exchange effects and provides the additional information that the anomalous overall ESR absorption of the 2-hydroxyprop-2-yl (2-propanolyl) radical is due to spin–lattice relaxation in the triplet acetone precursor. The effect is weakened in the photolysed acetone/triethylamine system because of the rapid reaction of photoexcited acetone with triethylamine, which results in reaction both *via* its singlet state, which cannot produce a net polarisation, and the triplet state, which yields no triplet polarisation, and reacts before spin–lattice relaxation can produce full equilibrium polarisation.[22] The frequency dependence of the electron spin relaxation rates ($1/T_{1e}$) of nitroxides has been measured by saturation-recovery in water/glycerol or water/sorbitol mixtures at room temperature at X-, S- and L-band frequencies (9.2, 3.1 and 1.9 GHz respectively). Tumbling correlation times were calculated from the CW X-band spectra. The dependence of T_{1e} on the tumbling correlation time of the probe was modelled from the modulation of the ^{14}N hyperfine and *g*-anisotropy, spin-rotational coupling, and from one or more thermally-activated processes. As expected at these frequencies, it is the modulation of the ^{14}N nuclear hyperfine anisotropy that provides the dominant relaxation pathway, with the *g*-anisotropy modulation somewhat less, and spin-rotation almost negligible. The contributions from the thermally-activated processes, and from modulation of the ^{14}N hyperfine interaction, increase as the frequency is reduced.[23] Simulations of EPR spectra from phospholipid-based probes, labelled at the C4 to C14 positions of the an-2 chain, in liquid-ordered membranes of dimyristoylphosphatidylcholine, containing 40 mol% cholesterol, measured at 94 and 9 GHz frequencies, have been presented.[24] The 94 GHz spectra could be satisfactorily simulated using motional narrowing theory, which accounts more effectively for averaging of the g_{xx}/g_{yy} components, with a restricted motion about the z-axis, than do slow-motion descriptions (Brownian and strong-jump). Polarity-correlated *g*-tensors are required for the high-field simulations, and are obtained from low temperature measurements (173 K). Full details are given of the procedures used to derive the spin Hamiltonian parameters, which are used in the stochastic Liouville equation to obtain the anisotropic parameters of the slow motional component, evident in the 9 GHz spectra. The rapid diffusional component is thought to be due to segmental motion of the lipid chains and the slow

diffusional component to angular fluctuations of the chain axis. The latter are not constant along the length of the chain, but rather increase in amplitude on progressing towards the methyl group terminus.[24]

Changing tack somewhat, an intriguing paper is concerned with a neutral radical derived from dodecyl syringate, which, it is suggested, may prove a good candidate for molecular ESR quantum computers. Quantum chemical calculations indicate that this molecule, with a stable delocalised unpaired electron spin, may represent a qubit in quantum information processing. I leave the interested reader to explore this argument in more detail.[25] I shall conclude this section with two more papers on theory and two more on practice. Firstly, I note that calculations have been made of the *g*-factors and hyperfine coupling constants for the Co^{2+} cation doped into a $CsMgCl_3$ crystal. The Co^{2+} centres possess a trigonal configuration, and the calculations were based on higher-order perturbation equations. The contributions from the effect of covalency and from the configuration interaction were considered, and the parameters pertaining to both were derived from optical spectra.[26] As an organic example, I cite a report on a theoretical study of the spin-trapping of the hydroxyl radical by cyclic nitrones using Density Functional Theory (DFT). From the energies obtained for the nitrones themselves and their OH-adducts, it was concluded that *trans* adduct formation is favoured in alkoxycarbonyl nitrones, while alkoxyphosphoryl nitrones prefer to form the *cis* adduct, since this is stabilised by intramolecular hydrogen bonding. Addition of hydroxyl to a phosphoryl-substituted nitrone is more exoergic than to carbonyl-substituted nitrones.

Dimethoxyphosphoryl substitution in a DMPO-type structure was found to be the most effective substitution site for trapping a hydroxyl radical.[27] Obviously, I am now pre-empting the next section on biological systems, and to complete the transition, I shall make mention of two papers on the use of aqueous flat cells oriented perpendicular to the electric field for use in ESR which detail their employment with a TE_{102} cavity to maximise sensitivity when using aqueous samples.[28,29] A practical multiple cell sample structure is proposed that yields 2.0–2.3 times the sensitivity compared with a single flat cell in the nodal orientation. The authors also describe a modified TE_{102} resonator design with square rather than cylindrical sample access stacks that is predicted to provide an enhancement factor of 2.2–2.7 in ESR signal intensity compared with a single flat cell in the nodal orientation.[29]

3. Biological systems

I commence this section with a distinctly biological example, that of the ESR imaging of nitric oxide in mice that had been treated with lipopolysaccharides. Male mice, each of around 30 g in weight, were injected interperitoneally with 10 mg kg^{-1} of lipopolysaccharide, and after six hours an NO trapping reagent, consisting of an iron *N*-dithiocarboxy sarcosine (DTCS) complex, was injected. Two hours later, the mice were restrained in a plastic holder and placed in an L-band loop-gap resonator operating at 1 GHz. The NO–$Fe(DTCS)_2$ complex was detected in the upper abdominal regions of these animals, and 3D images were obtained of this complex in the liver and kidney regions simultaneously. The NO–$Fe(DTCS)_2$ distributions were confirmed by homogenizing each organ and measuring the homogenate using conventional X-band ESR. This is apparently the first EPR image of NO in live mice kidneys to be made.[30] Another study describes taking ESR 'snapshots' of the oxidative stress status of the blood of a rather larger animal—the human. This

employed a novel EPR-based radical probe to measure directly the concentration of reactive oxygen species (ROS) in the peripheral blood of athletes and manual workers during a sixty minute period of controlled exercise. In this experiment, the probe material was bis(1-hydroxy-2,2,6,6-tetramethyl-4-piperidinyl)decandioate, chosen since it reacts quantitatively with oxygen-centred radicals, including superoxide, which oxidise it to the parent nitroxide. Presumably the presence of the two N–OH groups is a statistical device to increase the overall nitroxide yield, and the spacer decandioate group is sufficiently long that the spin-interaction between the two nitroxide groups in the bis-nitroxide biradical is weak, hence giving a simple ESR spectrum, effectively corresponding to that of a mono-nitroxide. Interestingly, the measurements suggest that people who are normally active (*e.g.* through their work) may benefit while they are at rest, more than athletes do from antioxidant supplementation; however, during exercise, it is athletes who may obtain the greater benefit from antioxidant administration.[31] Since free radical-induced oxidative stress has been implicated in the pathogenesis of oral diseases such as periodontitis and temporomandibular joint disease, among the many, a study was made of nitroxide spin probes such as 3-carbamoyl-2,2,5,5-tetramethylpyrrolidine-1-oxyl (carbamoyl-PROXYL) in the head region of live mice using a 3D imaging system. It was found that the probe could be detected down to a concentration of 0.25 mM. The authors suggest that this approach of *in vivo* ESR imaging might be used in the non-invasive assessment of free radical-induced oxidative stress in oral diseases using small animal models.[32] An overview is presented of aspects of *in vivo* EPR spectroscopy, including potential diagnostic applications. Specifically considered are the measurement of nitric oxide and of oxygen in living systems, mainly in regard to their role in septic shock, utilising a murine (mouse) model developed in the laboratory of the authors, based in Cardiff. In their work, oxygen concentrations are measured in terms of oxygen pressure (pO_2), as is usual in biology, using the particulate probes LiPc (Lithium Phthalocyanine) and ''Gloxy'', which are surgically implanted at specific sites in tissues. The name Gloxy is derived from the Welsh word for coal ''glo''; the suffix ''oxy'' is obvious given its application. As a soluble probe, trityl (a water soluble derivative of the triphenylmethyl radical, in fact) is administered intravenously. Nitric oxide is measured as the NO–Fe(DETC)$_2$ complex (DETC = DiEthyldiThioCarbamate), following the administration of Fe^{2+} and DETC.[33] The determination of nitric oxide in biological samples has been reviewed. It is pointed out that the particular properties of NO enable it to be detected specifically from all other molecules. A summary is made of the various methods that have been employed successfully to detect NO, including gas and liquid phase chemoluminescence, ESR spectroscopy combined with spin trapping (of the kind we have seen in the above examples), UV/visible spectroscopy and fluorescence (spectrophotometric methods), electrochemical sensors, and reporter cell assay. The basis, applications, merits and limitations of each method are considered.[34] Another review outlines the oxidative stress-induced formation of ROS and consequently other radicals, and protective mechanisms to militate against this. The formation of these species from a model system that incorporates Cu(II) complexes and H_2O_2 is described, as is the development of radical scavengers for active oxygen and other radicals, for example oligopeptide–Cu(II) complexes. NO trapping agents are considered along with their applications, and the non-invasive evaluation of X-ray radiation-induced damage and oxidative stress using *in vivo* ESR and ESR imaging.[35]

A model system has been devised to evaluate the possible relationship between the degree of blood oxygenation and cerebral tissue pO_2 *via* a mouse model, using LiPc

as the oxygen probe. Over the period of the evaluation, both cerebral tissue and blood pO_2 were found to fall due to the depressive effects of anesthesia on the respiratory and circulatory centres of the brain. Cerebral tissue showed slight less total decrease in pO_2 compared to blood, and average pO_2 levels were maintained at around 55 mmHg for up to 130 min. Cerebral pO_2 values, obtained using LiPc in the mouse brain, were found to be the same as previously measured in rat brain, with values close to 51 mmHg in non-anesthetized animals and about 49 mmHg in those anesthetized with Ketaset.[36] In an *in vitro* study, the possible cooperation between α-tocopherol and zeaxanthin might act synergetically to protect against photosensitised lipid peroxidation, mediated by singlet oxygen and free radicals. The antioxidative action was studied in liposomes made from phosphatidylcholine and cholesterol. The progress of lipid peroxidation, induced by photoexcitation of rose bengal in the presence of air, was monitored by the detection of lipid peroxides and by ESR oximetry. Cholesterol served the mechanistic function of being converted to reporter molecules, since it forms characteristic products of its reactions with singlet oxygen or with free radicals. It was found that zeaxanthin alone (even at concentrations of 2.5 μM) could efficiently protect against singlet oxygen-induced lipid peroxidation but that it was rapidly consumed by reaction with free radicals. α-Tocopherol alone was ineffective in preventing lipid peroxidation, even at a concentration of 100 μM. However, in combination, zeaxanthin and α-tocopherol were found to act synergistically, and this may be explained in terms of preventing the carotenoid from being consumed by radicals, which are instead intercepted by α-tocopherol, thus leaving the zeaxanthin available to quench the primary singlet oxygen species effectively.[37] It has been shown that mM concentrations of sodium fluoride (NaF) induced cell death by apoptosis, characterised by caspase activation and DNA fragmentation in tumour cell lines. Further work has demonstrated that the activity of NaF is neither enhanced nor protected-against by a range of antioxidants, oxidants, metals or saliva, as present in non-cytotoxic concentrations, whereas at cytotoxic levels, a somewhat additive, although not synergistic, effect on the cytotoxic influence of NaF was found. ESR measurements demonstrated that NaF did not change the radical intensity of the ascorbyl radical signal, measured from a mixture of sodium ascorbate and gallic acid under alkaline conditions. It is proposed that the cytotoxic effect of NaF is not regulated by a redox mechanism, but rather by a rapid decline in glucose concentration at an early stage.[38]

In order to model the mononuclear Fe(III)–OOH species identified in the catalytic cycle of the anti-cancer drug bleomycin, the complex between Fe and the pentadentate ligand *N*-[bis(2-pyridylmethyl)aminoethyl]pyridine-2-carboxamide (H-$PaPy_3$), [Fe(III)($PaPy_3$)OCH_3](ClO_4), was reacted with H_2O_2 to form a red species (λ_{max} = 480 nm, ε = 1800 M^{-1} cm^{-1}), with a $S = \frac{1}{2}$ ESR signal showing *g*-values of 2.25, 2.17 and 1.95. The species was identified by electrospray mass spectrometry as [Fe(III)($PaPy_3$)OOH)](ClO_4). The decomposition of the complex results in the modification of the ligand, in which one H atom is replaced by a CH_3O group from the solvent. The substitution is a result of a two-electron oxidation of the ligand following heterolytic cleavage of the O–O bond of the Fe–OOH species, and is a plausible mechanism from which to rationalise the related ligand modifications that are proposed to occur in the decay of bleomycin.[39] A series of DFT calculations were made to predict the ^{57}Fe Mössbauer quadrupole splittings (ΔE_Q) and isomer shifts (δ_{Fe}) of a Fe(IV):O model compound: [Fe(O)(TMC)(NCMe)]$(OTf)_2$, where TMC = 1,4,8,11-tetramethyl-1,4,8,11-tetrazacyclotetradecane and OTf = $CF_3SO_3^-$. A cytochrome P450 reaction intermediate was also investigated. Good agreement with

experimental parameters was obtained, particularly for the model compound.[40] A direct determination was made of the number of electrons required to reduce Coenzyme F430 pentamethyl ester to the Ni(I) species that displayed EPR and UV/visible spectra characteristic of the MCR_{RED1} state of methyl-coenzyme M reductase using electrolytic methods. It is demonstrated that the step is, in fact, a one-electron process, and is therefore inconsistent with reduction of the macrocycle chromophore.[41] A determination of the tertiary structure of RNA has been reported from ESR measurements of the hammerhead ribozyme, composed of one core and three helices, whose configuration depends on the concentration of magnesium. The absence of a natural unpaired electron, of course, imposes a considerable restriction on the use of ESR for their structural investigation, and the lack of a strongly-coupled magnetic nucleus in high abundance is a further limitation. As is demonstrated in this work, these limitations may be circumvented by introducing two spin labels so that distances between them can be determined by pulsed electron double resonance measurements. To obviate the latter restriction, the Mg ions may be replaced by Mn, with nuclear spin $I = \frac{5}{2}$, thereby acting as a direct probe of the coordination environment.[42] The proton-pumping NADH:ubiquinone oxidoreductase, for simplicity also known as respiratory complex I, couples the transfer of electrons from NADH to ubiquinone with the transfer of protons across the membrane. Up to nine iron-sulfur (Fe/S) clusters are known to participate in this redox reaction. There is some discussion that the EPR-detectable cluster N2 is involved in proton pumping. However, the assignment of this cluster to a distinct sub-unit of the complex, in addition to the matter of exactly how many Fe/S clusters actually give rise to the EPR signal, remains a matter of debate. Complex I, from *Escherichia coli*, consists of thirteen polypeptides designated NuoA–NuoN. Either sub-unit, NuoB or NuoI, could contain cluster N2. From a series of mutation experiments, it is concluded that the Fe/S cluster N2 is actually located on sub-unit NuoB.[43]

Tyrosine (Y_D) in the D2 reaction centre of photosystem II (PSII) is redox-active and, under illumination, forms a radical ($Y^{\bullet}_D$) that is stable in the dark, although neither the origin of its stability nor its functional role are well understood. Since there is considerable variation in the literature of reported hyperfine coupling data for ($Y^{\bullet}_D$), it is essential to make an unambiguous assignment of this species. To address this task, the hyperfine structure of the tyrosine radical ($Y^{\bullet}_D$) in PSII was probed by EPR spectroscopy, in conjunction with site-specific isotope labelling. A comprehensive series of different selectively ^{2}H-, ^{13}C- or ^{17}O-labelled tyrosine isotopomers was synthesised and incorporated into *Spirodela oligorrhiza*, obtaining an enrichment of greater than 95%. The ^{13}C and ^{17}O interactions were obtained using spectral simulations. From the anisotropy in the hyperfine interactions, the spin densities at all phenoxyl ring positions were measured precisely. From a comparison between ($Y^{\bullet}_D$) and the parent tyrosine radical, as measured in a glassy matrix, it is concluded that there is a well-ordered hydrogen bond present between ($Y^{\bullet}_D$) and the surrounding matrix, with a bond length of 1.5 Å. Enantioselective labelling confirms that the β-methylene H-atoms of ($Y^{\bullet}_D$) in *Spirodela oligorrhiza* are oriented in a highly constrained, specific position that strongly immobilises the radical, thereby ensuring the formation of a firm hydrogen bond between the phenoxyl oxygen atom and the protein matrix.[44] The frozen solution ESR spectrum of the primary donor cation $P^{+\bullet}$ in reaction centres of site-directed mutants of *Rhodobacter sphaeroids* (Rb.) has been obtained at a microwave frequency of 360 GHz and a magnetic field strength of 12.8 T. Due to the high Zeeman resolution of

the powder pattern measured at 160 K, all three components of the rhombic *g*-tensors could be measured with a high accuracy, providing novel structural information about these complexes.[45] The photogeneration of hydroxyl radicals by PSII membranes has been investigated by spin-trapping with the POBN trap. Two kinetically distinct phases were observed in the production of the HO–POBN spin-adduct, and were distinguished by half lives of 7.5 min for the first phase and 30 min for the second one. The generation of hydroxyl radicals was found to be suppressed when the Mn complex was absent, but could be restored by the addition of an artificial electron donor (DPC). The absence of oxygen also caused a suppression of hydroxyl radical production, but the reintroduction of oxygen restored it. From the overall pattern of results obtained, it was concluded that hydroxyl radicals are produced on the electron acceptor side of PSII by two different routes. In one, superoxide, generated by reduction of O_2, interacts with a PSII metal centre, most likely the non-heme iron, to form an iron–peroxide species that is further reduced to hydroxyl radical by an electron from PSII, presumably *via* Q_A^-. In the second route, superoxide is thought to dismutate to form free H_2O_2, which is then reduced *via* the Fenton reaction with metal ions, of which the most likely are Mn^{2+} and Fe^{2+}, released from photodamaged PSII.[46] X-band ESR and electronic absorption spectra were recorded from the recently synthesised imidazolate-bridged heterobimetallic complexes [(tren)Cu-E-Im-Zn-(tren)]$(ClO_4)_3$ and [(tren)Cu-E-Im-Ni-(tren)]$(ClO_4)_3$ (where tren = tris(2-aminoethyl)amine and E-Im = 2-ethylimidazolate ion), and the related mononuclear complexes [Cu(tren)]$(ClO_4)_2$ and [(tren)-Cu-ImH]$(ClO_4)_2$. The biological activities of these complexes (towards superoxide dismutase and their antimicrobial action) were also measured and compared with their molecular properties.[47] Procyanidin B2 (epicatechin-(4β-8)-epicatechin) is present in grape seeds, apples and cacao beans, and has antioxidant properties. Spin trapping with TEMPO demonstrated that procyanidin B2 decreased the signal intensity of the OH–TEMPO adduct formed in a Fe(II)/H_2O_2 system, while, in contrast, it caused an enhancement in the signal when Cu(II)/H_2O_2 was used to generate hydroxyl radicals. Results from UV/visible spectroscopy showed that procyanidin B2 chelates Fe(II), which may be related to its antioxidant function. DNA damage was also measured in human subjects who had consumed procyanidin B2. Taken together, the results indicate that this material may exert both antioxidant and prooxidant behaviour by interacting with H_2O_2 and metal ions.[48] Research into radiation damage to DNA remains active, although I have found fewer papers on this general subject this time than was the case perhaps ten or so years ago. In a recent review, Sevilla considers the mechanisms of hole formation and electron transfer processes in DNA that has been irradiated at low temperatures. It is shown that DNA is a very efficient electron trap, scavenging 30–60% of all electrons and holes that are formed by the action of ionising radiation upon it. Electrons are trapped at the pyrimidine bases, cytosine and thymine, whereas holes are trapped mainly on guanine. Results show that all electrons in the hydration layer are transferred to DNA and all holes in the first layer of water also transfer to DNA; in contrast, holes in the subsequent layers tend to form hydroxyl radicals. After trapping, electron migration and hole transfer processes within DNA at low temperatures are limited to tunnelling events. ESR studies have followed the time-dependent transport of electrons and holes from DNA to acceptors such as intercalators or modified bases. Electron transfer through the DNA stack and between duplexes has been elucidated, in addition to the effects of DNA hydration, complexing agents, base sequence, and H/D isotope exchange on electron transfer

distances and rates. By means of variable temperature studies, a discrimination is possible between tunnelling and the thermally-activated processes which dominate at temperatures near and above 200 K.[49] There is a very interesting and potentially important paper which describes the type of damage that is induced in DNA by different kinds of ionising radiation, namely X-rays, protons and α-particles. Single crystals of anhydrous thymine and cytosine monohydrate were irradiated at room temperature using X-rays, 20 MeV protons and 35 MeV α-particles, and the relative distributions of the various stable, radiation-induced radicals were determined using ESR. Since the ESR spectra of the individual radicals had previously been obtained, the composite spectra could be reconstructed using a fitting procedure, and hence their relative amounts quantified. It was found that the relative yields varied according to the kind of radiation, with the most prominent differences being between X-rays and either form of particulate radiation.[50]

The effect of forced, chronic swimming training and enriched chow containing 1% wt/wt dried nettle (*Urtica dioica*) leaf were investigated for oxidative stress, inflammation and neurotrophic markers in Wistar rat brains. The rats were divided into groups and subjected to swimming training for six weeks or to nettle supplementation for eight weeks or to a combination of both these treatments. The level of oxidative stress was measured by ESR and by the concentration of carbonylated proteins. The conclusions from this study were that nettle supplementation reduces the concentration of free radicals in both the cerebellum and frontal lobe regions. Swimming, however, did not influence significantly the oxidative damage. It appears that both nettle supplementation and swimming influence physiological brain functions. Nettle was found to be an effective antioxidant and possible antiapoptotic agent, prolonging the lifetimes of brain cells, and it is suggested that exercise may also play a role in antiapoptotic processes, which are important following brain injury.[51] The interaction of hypochlorite with linoleic acid hydroperoxide was studied using chemiluminescence and ESR spin-trapping with POBN. It was shown that the addition of hypochlorite to an incubation media containing linoleic acid and lipoxygenase resulted in an intense chemiluminescence flash, which correlated with the hydroperoxide concentration. It is thought that a peroxyl type radical is trapped by POBN along with a carbon-centred radical. The data suggest that hypochlorite produced in phagocytes can induce the production of both oxygen- and carbon-centred free radicals as promoters of free radical processes.[52]

A review has been published concerning intermediates produced in cytochrome P450 catalysis. Cytochromes P450 (plural, since it is a "family" of enzymes) are enzymes that catalyse the insertion of a single O_2-derived O atom into an unactivated C–H bond, and are therefore potent oxidants. A sophisticated arsenal of EPR, ENDOR and more traditional methods of absorption spectroscopy have been able to identify key reaction intermediates, while crystallography has defined the structures of the substrate-free, substrate-bound and oxy complexes. Despite this extensive range of information, the nature of the Fe(IV):O intermediate, thought to be the active oxygen transfer agent, has remained elusive, and theoretical methods (especially DFT) have provided valuable insights in this regard.[53] I also note a book chapter published on the subject of theoretical calculations in P450 catalysis.[54] The triplet states of PSII core particles, extracted from spinach, were studied using time-resolved EPR at different reduction states of the iron–quinone complex of the reaction centre primary electron acceptor. When the reaction centre was doubly-reduced, the well known PSII triplet state, characterised by the zero-field splitting parameters $|D| = 0.0286$ cm^{-1} and $|E| = 0.0044$ cm^{-1}, was detected. When the

primary acceptor was singly-reduced, a triplet state of a different spectral form but with identical D and E parameters was produced, and with a characteristic spin polarisation pattern arising from radical pair combination. The latter triplet state was strongly temperature-dependent, and disappeared at a temperature of 100 K with a much faster decay than was found for the other triplet. This rapidly decaying state was ascribed to the PSII reaction centre. A sequence of electron transfer steps in the reaction centres is proposed, accounting for the dependence of the triplet state features on the reduction state of the iron–quinone primary acceptor complex.[55] In another study, the proximity of the calcium/strontium binding site of the oxygen-evolving complex (OEC) in the paramagnetic Mn cluster of PSII is probed by means of ^{87}Sr three-pulse electron spin-echo envelope modulation (ESEEM) spectroscopy. No signal was detected when Sr was used in natural abundance (7% ^{87}Sr), but enrichment to 93% of this isotope resulted in clear modulation, arising from the $I = {}^{9}/_{2}$ ^{87}Sr nucleus, which is weakly coupled to the Mn cluster. Using a simple point dipole approximation analysis, a Mn–Ca(Sr) distance of 4.5 Å is suggested. When a more appropriate model was used, the 4.5 Å average was transformed into a distance range of 3.8–5.0 Å. The result provides independent evidence that the calcium/strontium binding site is close to the Mn cluster in the OEC of PSII.[56] Using ESR detection and spin-trapping of hydroxyl radicals with DMPO, it has been shown that manganous ions can substitute for iron or copper ions in a Fenton system. HPLC with fluorescence detection was used simultaneously to measure hydroxyl radical production in this system. L-Phenylalanine is converted to the highly fluorescent L-tyrosine in the presence of hydroxyl radicals, and can be used as the fluorescence probe for their formation.[57] When a DMSO (dimethylsulfoxide) solution of lignin extracted from softwood was heat-treated in the presence of the spin-trap 2,4,6-tri-*tert*-butylnitrosobenzene at about 40 °C, spectra from secondary carbon-centred radicals ($R_2CH^{\bullet}$) were recorded, demonstrating the homolytic cleavage of alkyl aryl ether bonds, R–O(aryl). At about 60 °C, three kinds of radicals were detected, primary ($RCH_2^{\bullet}$), secondary ($R_2CH^{\bullet}$) and tertiary ($R_3C^{\bullet}$).[58] I end this section with two papers, one of which reports an investigation of free radicals produced in the tar and gas phases of mainstream cigarette smoke using spin-trapping. Among the different kinds studied, it appears that oriental cigarettes give the highest yield of free radicals.[59] In the second paper, the bioabsorption of Cu^{2+} ions by dried leaves was determined by FT-IR and ESR. Cu^{2+} ions in the biomass affect the IR bands corresponding to C=C vibrations of the carbon rings present therein, while the ESR spectra show that they are coordinated into the biomass in a state of axial symmetry. A model is proposed for the absorption sites, in which Cu^{2+} are located between two adjacent carbon rings in an interstitial site in the leaf fibres.[60]

4. Organic radicals

Spin trapping and radical reactivity

I shall start this section with reports of some chemical systems whose methodology might, in principle, be used later in studies of actual biological systems. Therefore, while there is some overlap with the considerations of the previous section, as the actual systems investigated currently rest within the realm of "organic chemistry", I have included them here. For example, it has been demonstrated that aci-anions of nitroalkanes, formed by rearrangement of the parent compounds in alkaline solutions, are efficient spin-traps for nitric oxide. The general structure of the adduct under strongly basic conditions is $RC(NO)NO_2^{\bullet 2-}$ (0.5 M NaOH) and with alkaline

buffers (pH 10–13) it is $RCH(NO)NO_2^{\bullet -}$. The hyperfine splitting from ^{14}N in the NO_2 moiety (11.2–12.48 G) and that from the trapped NO moiety (5.23–6.5 G) are quite distinct from each other. The structure of the adducts was confirmed by using ^{15}NO, which produced radical adducts in which the triplet structure from trapped ^{14}NO ($I = 1$) was replaced by a doublet structure from ^{15}NO ($I = \frac{1}{2}$). In the case of the aci nitromethane/NO adduct, it was found that in 0.5 M NaOD, the hydrogen at the α-carbon could be substituted by deuterium, giving the $CD(NO)NO_2^{\bullet 2-}$ radical. It is suggested that methodologies for NO trapping in biological systems might be developed along these lines, but given the pH requirements, it is hard to see how.[61] Water soluble trityl type probes (substituted triphenylmethyl radicals) have been reported as suitable for use in the measurement of superoxide. The particular radical, TAM OX063, is highly soluble in water and shows a single very sharp ESR line in aqueous media. It is also highly stable (as expected), even in the presence of many oxo reductants such as ascorbate and glutathione that are present in biological systems. TAM reacts with superoxide with an apparent second-order rate constant of 3.1×10^3 M^{-1} s^{-1}. The specific reactivity of TAM towards superoxide, which causes the loss of the ESR signal, was used to detect the generation of superoxide in various model systems. The changes in the linewidth, induced by Heisenberg exchange with paramagnetic oxygen, were utilised to determine simultaneously the consumption of oxygen during the reactions occurring in the model systems. The effect of the flux of superoxide and the concentration of TAM on the efficiency of superoxide detection were also investigated.[62] In a following paper by the same group,[63] a spectrophotometric method is proposed to measure the reaction between TAM and superoxide that takes advantage of the newly formed and distinct absorption peak corresponding to the product formed from the reaction between these two species. The effects of different fluxes of superoxide and TAM concentrations were studied and compared with the more widely used cytochrome c method of superoxide detection. The authors conclude that the two methods are comparable, and that the spectrophotometric method further complements the ESR assay.[62] The spin-trap EPPN [*N*-2-(2-ethoxycarbonyl-propyl)-α-phenylnitrone] has been reported to form a superoxide spin-adduct ($t_{\frac{1}{2}} = 5.25$ min at pH 7.0) that is considerably more stable than the corresponding adducts of superoxide with (the related) *N-tert*-butyl-α-phenylnitrone ($t_{\frac{1}{2}} = 10$ s) or DMPO ($t_{\frac{1}{2}} = 45$ s). In an effort to optimize the chemical structures of EPPN-type traps, a series of six different EPPN derivatives was synthesised and characterised using ^1H and ^{13}C NMR and IR spectroscopy. The ethoxy group in EPPN was replaced by propoxy-, *iso*-propoxy-, *n*-butoxy-, *sec*-butoxy- and *tert*-butoxy- groups, and then the phenyl group was substituted by a pyridyl group. Cutting a long story short, no improvement was found when the ethoxy group was replaced by other substituents, and some of the derivatives led to decomposition products.[64] Using Transition State Theory, experimental rate constants, determined over a range of temperatures, for reactions of vitamin E-type antioxidants were analysed in terms of their enthalpies and entropies of activation. Using semi-empirical methods (PM3), the overall reaction enthalpies and entropies, and hence Gibbs free energies, for reactions of vitamin E-type antioxidants were determined, whose rate constants had been determined at a single temperature. Within the linear free energy relation (LFER) assumption, where the Gibbs free energy of activation is proportional to the overall Gibbs free energy change for the reaction, it is possible to rationalise, and even to predict, the relative contributions of enthalpy and entropy for reactions of interest involving potential antioxidants. An experimental method was also devised, involving a competition between $^{\bullet}CH_3$

radicals reacting with the spin trap PBN and with the antioxidant, which enables the relatively rapid determination of a relative order of activities for potential antioxidant compounds, and also their rate constants for scavenging $^{\bullet}CH_3$ radicals (relative to the rate constant for the addition of $^{\bullet}CH_3$ to PBN).[65] In a related approach to evaluating antioxidant activities, rate constants were determined for the reaction of antioxidant species with the hydroxyl radical using a rapid-flow ESR method. When an antioxidant and ethanol were present together, a competition occurred for reaction with $HO^{\bullet}$, such that the spectrum of the 1-hydroxyethyl radical was superimposed upon that of the antioxidant-derived radical. The intensity ratio of the two kinds of radicals was determined from a double integration of the two sets of signals, which yielded directly the ratio of the rate constants for the reactions of $HO^{\bullet}$ with the antioxidant and with ethanol, expressed as the rate ratio (antioxidant : ethanol). Thus, the following ratios were obtained: pyrogallol (19 : 1), gallic acid (17 : 1), catechol (11 : 1), phloroglucinol (1.5 : 1), resorcinol (1.2 : 1) and methanol (0.56 : 1). The dissociation energies of the O–H bonds in the antioxidant molecules were predicted by MO calculations. The relationship between the relative activation energies, obtained from the rate constants, and the bond dissociation energies shows that the Evans–Polanyi equation holds across the polyphenol series but that the line for the alcohols is shifted from this. It is thought that the structures of the transition states for the alcohols are stabilised by a polar effect.[66] The O–H bond dissociation enthalpies (BDEs) of a series of thirteen oximes ($R_2C{=}NOH$) have been reported. Experimental anchor points used to validate the results of theoretical calculations include: (1) the O–H BDEs of $Bu^t{}_2C{=}NOH$, $Bu^tPr^iC{=}NOH$ and Bu^t(1-adamantyl)C=NOH (determined previously from the heat released in the reaction between $Bu^t{}_2C{=}NO^{\bullet}$ and PhNHNHPh in benzene), all of which were decreased by 1.7 kcal mol^{-1} to reflect a revision to the heat of formation of (*E*)-azobenzene (which, in fact, has significant implications for other BDEs) and to correct for the heat of hydrogen bonding of $Bu^t{}_2C{=}NOH$ to benzene (0.43 kcal mol^{-1}); (2) the measured rates of thermolysis of six $R_2C{=}NOCH_2Ph$ derivatives at 423 or 443 K, which were used to derive O–H BDEs for the corresponding $R_2C{=}NOH$ molecules. It is noted that previous claims that the O–H BDEs in mono- and diaryloximes are significantly lower than are those for alkyloximes, due to delocalisation of the unpaired electron into the aromatic ring, have always been at odds with the known structures of iminoxyl radicals, as are the purported "perpendicular" structures (*i.e.* N–O pointing out of the C_2–N plane) of sterically-hindered radicals. The present results confirm a conclusion drawn in 1973 that simple steric effects rather than spin-delocalistion or drastic geometrical changes are responsible for the relatively minor differences in oxime O–H BDEs.[67]

Another group has investigated the benzotriazole-*N*-oxyl radical (BTNO), formed by oxidising 1-hydroxybenzotriazole with a Ce^{4+} salt in acetonitrile solution. BTNO is characterised by a broad absorption band with $\lambda_{max} = 474$ nm and $\varepsilon = 1840\ M^{-1}\ cm^{-1}$, and its spontaneous decay with a first-order rate constant of $6.3 \times 10^{-3}\ s^{-1}$ in MeCN at 25 °C. This decay is strongly accelerated by the presence of H-donor substrates such as alkylarenes, benzyl and allyl alcohols, and alkanols, for which rate constants of the H-abstraction reactions were measured. The kinetic isotope effect confirms that the H-abstraction step is rate-determining, and activation parameters were measured in the range 15–40 °C for selected substrates. A correlation between the activation energy and BDE(C–H) for a small series of H-donors was obtained according to the Evans–Polanyi equation, giving $\alpha = 0.44$. The plot enables the

experimentally unavailable BDE(C–H) in benzyl alcohol to be determined by extrapolation as 79 kcal mol^{-1}.[68]

The matter of "captodative stabilisation" in radicals continues to provide some interest. In a captodative system, the combined effect of a donor and an acceptor substituent exert a greater combined influence than the simple sum of their individual effects. It is possible that substituents of the same kind, *i.e.* both donors or both acceptors, may act antagonistically. Adam has reported the measurement of the EPR zero-field parameter $|D|$ in a series of substituted triplet biradicals **1**, isolated in a 2-methyltetrahydrofuran matrix at 77 K, so as to probe the electronic substituent effects on the spin density distribution in the system (*i.e.* the more spin-delocalisation there is by the substituents X and Y, the smaller is $|D|$). A parameter, ΔS, is calculated from the ESR data and used to express whether the substituents X and Y are acting additively, synergistically or antagonistically. In this study, it was found that pairs of electron donor substituents act antagonistically, while pairs R_2N/electron acceptor and MeO/electron acceptor show synergistic delocalisation of spin-density. In contrast, MeS/electron acceptor pairs manifest only an additive behaviour. The results are explained in terms of the appropriate electron transfer-type mesomeric structures.[69]

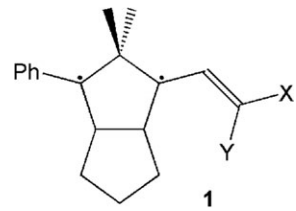

1

The catechin derivative **2** (formed by the reaction of (+)-catechin (**3**) with acetone in the presence of $Et_2O{:}BF_3$), in which the catechol and chroman rings are forced to be planar, shows an enhanced protective effect against DNA oxidation without the prooxidant effect shown by **3**. Studies were undertaken in order to further examine the radical scavenging ability of **2** in its reaction with the cumyl peroxyl radical ($PhCMe_2OO^{\bullet}$), since this is a model for lipid peroxyl radicals in lipid peroxidation. The kinetics of H-atom transfer from **2** and **3** to $PhCMe_2OO^{\bullet}$, measured in propionitrile, show that the rate of H-atom transfer from **2** is significantly faster than it is from **3**, and it is interesting that the rate was accelerated in the presence of $Sc(O_3SCF_3)_3$. Such an effect of the presence of a metal ion indicates that the hydrogen transfer reaction proceeds *via* metal ion-promoted electron transfer from **2** to the peroxyl radical, followed by a H-transfer, rather than *via* a one-step H-atom transfer. The electrochemical activity of **2** towards a one-electron oxidation (more negative oxidation potential), investigated by second-harmonic a.c. voltammetry, strongly supports the two-step mechanism for an overall H-atom transfer, and resulting in an enhanced radical scavenging ability over **3**.[70] Absorption spectrophotometric studies indicated that, in chloroform solution, β-carotene reacted with NO_2 with a stoichiometry of 1 : 2. To understand the mechanism of this reaction, free radical intermediates produced during the reaction were spin-trapped using 2-methyl-2-nitrosopropane (MNP) and 4-pyridyl-1-oxide-*N*-*tert*-butylnitrone (POBN), the spin-adducts of which were detected by ESR. NO_2 alone did not react with the spin traps, but the introduction of β-carotene resulted in the production of

different radicals that could be identified according to their ^{1}H and ^{14}N hyperfine coupling constants. Two possible pathways exist for the reaction between NO_2 and β-carotene, *viz*. electron transfer and addition to the polyene chain. The present results supported the production of radicals by addition, yielding carbon-centred NO_2-β-carotene type radicals.[71] A report has appeared of the synthesis and structure of a novel spin-trap designed for trapping superoxide, 5,5-diethoxycarbonyl-1-pyrroline-*N*-oxide (DECPO). It was found that easy ESR detection of the HOO–DECPO adduct could be made, even when the concentration of superoxide was low. In comparison with DEPMPO (5-diethoxyphosphoryl-5-methyl-1-pyrroline-*N*-oxide), the trapping occurred at a faster rate, and also the detection of the HOO–DECPO adduct could be accomplished using a very low concentration of trap (0.5 mM).[72]

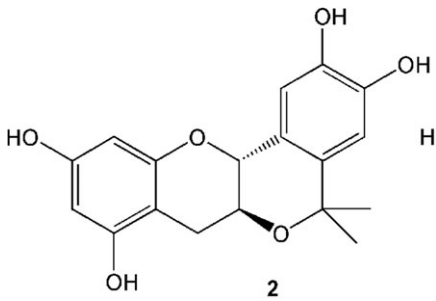

2

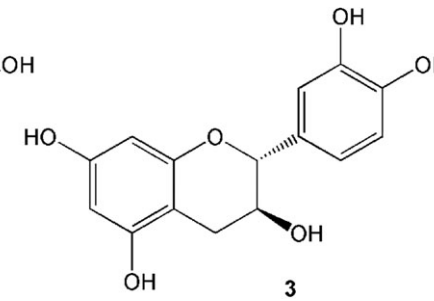

3

Triplets and radical pairs

By using time-resolved ESR, the quenching mechanisms of S_1 and T_1 coronene by TEMPO (2,2,6,6-tetramethylpiperidine-1-oxyl) were investigated on the basis of their absorptive and emissive chemically-induced electron polarisations (CIDEP), generated by the interactions of S_1 and T_1 states of coronene, respectively. Absolute magnitudes of the CIDEPs created on TEMPO radicals were determined as 1.8 (absorption) and 2.2 (emission), in the units of Boltzmann polarisation, by means of the Bloch equations. The overall results show that the T_1 component of coronene in benzene is quenched through an electron exchange interaction in an encounter complex. The difference between the magnitudes of the absorption and emission CIDEPs implies that the mean interaction distance of S_1 quenching is about 1–2 Å longer than that for T_1 quenching. This result suggests that a S_1–T_1 enhanced intersystem crossing occurs through both charge transfer and exchange mechanisms, while T_1 quenching occurs through exchange only.[73] The same group have investigated the interaction between the lowest excited singlet state of molecular oxygen, $O_2(^1\Delta_g)$, and TEMPO in benzene using time-resolved ESR. It is confirmed that the observation of absorption CIDEP is created through the interaction between $O_2(^1\Delta_g)$ and TEMPO. The absolute magnitude of the absorption CIDEP is estimated to be 340 ± 40 in units of the Boltzmann polarisation, and is one of the highest magnitudes of CIDEP so far measured by the time-resolved ESR method. The origin of this unusually large CIDEP is attributed to the large spin relaxation effect *via* the electron–electron spin-dipole interaction of $O_2(^3\Sigma_g^-)$, formed by the quenching of the $(^1\Delta_g)$ state of molecular O_2 by TEMPO.[74]

An analytical procedure is reported for the detection of peroxynitrite. The method involves the decomposition of peroxynitrite at physiological pH to yield a hydroxyl radical, which is ''trapped'' by reaction with DMSO, forming a free $^{\bullet}CH_3$, which is

then trapped with a spin-label fluorophore nitroxide-linked naphthalene (NTEMPO). This is a carbon-centred radical probe with a low fluorescence intensity which is transformed into a stable diamagnetic *O*-alkoxylamine, a high fluorescence compound. The fluorescence increment was proportional to the concentration of the hydroxyl radical and hence to the concentration of peroxynitrite.[75] It has been reported that ester-containing nitrones, including **4**, provide robust spin-traps for superoxide. The two enantiomers of **4** have been isolated using a chiral column. Using enantiomerically pure *S*- and *R*- forms of **4**, it was explored whether one of these isomers was solely responsible for trapping superoxide. The result was there was no difference in either ESR spectral parameters or adduct lifetimes, and neither in the ratio of *cis* to *trans* isomers formed.[76] It was shown that the one electron oxidation of compounds **5** and **6** occurs by a proton-coupled electron transfer mechanism to produce a phenoxyl radical hydrogen-bonded to an imidazolium carbon atom. Thus, these compounds serve as analogues of tyrosyl $D^{\bullet}$ in PSII. This structural conclusion was drawn from a combination of W-band EPR measurements and DFT calculations.[77]

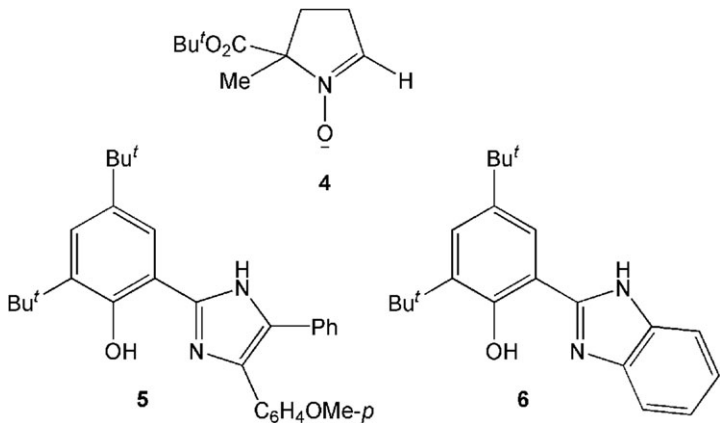

The photolysis of 2,4,6-triazido-1,3,5-triazine (cyanuric triazide (**7**)), as isolated in a solid matrix, has been studied. The stepwise generation of the corresponding mononitrene, dinitrene and trinitrene was observed by IR and ESR spectroscopy. The formation of the trinitrene, 2,4,6-trinitreno-1,3,5-triazine, as a septet state was confirmed for the first time by EPR spectroscopy. The trinitrene was readily decomposed into three NCN molecules upon further irradiation, as confirmed by matrix EPR spectroscopy.[78]

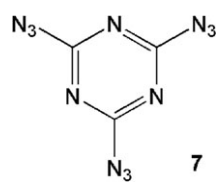

The photodynamic properties of three synthetic anthraquinone derivatives are reported, in terms of their relative efficiency to generate singlet oxygen, using both the *N*,*N*-dimethyl-4-nitrosoaniline bleaching assay and the ESR 2,2,6,6-tetramethyl-4-piperidinol assay (converted to the nitroxide). ESR is also used to detect spin-

adducts formed during the photodynamic action of these compounds under the particular conditions described.[79] Inverted (absorption/emission) chemically-induced dynamic electron polarisation (CIDEP) has been observed for random encounters of radical pairs, such as the phenoxyl radical with either e^-_q or the benzoate radical anion. A number of experiments have been undertaken in order to clarify the relationship between the energetics of the reactions of oxidising or reducing radicals and CIDEP behaviour. Inverted CIDEP is clearly the result of a change in the normal energy ordering of radical pair states so that the triplet state is lower.[80] The reaction kinetics of lithium metal with benzil in tetrahydrofuran (THF) were determined using a combination of GC product analysis and ESR measurements of the radical anion intermediates. The first radical anion intermediate, formed by chemisorption of the benzil onto the metal surface, was fully characterised and determined quantitatively from its ESR spectrum. A unique feature of this reaction is the existence of a well-defined and reproducible induction period. A mechanism is proposed which accounts for the main experimental observations.[81] The intramolecular electron transfer (ET) rates of a radical anion of dione **8** in *N*,*N*-dimethylformamide (DMF), acetonitrile (AN) and THF were determined at various temperatures using an ESR line-broadening method. Cryptand [2.2.2] (4,7,13,16,21,24-hexaoxa-1,10-diazabicyclo[8.8.8]-hexacosane) was added to the solutions in order to eliminate the counterion effect on the ET rates, caused by the presence of the sodium cation, produced in the chemical reduction to produce the radical anion. In DMF the rate constant was 1.5×10^{10} s^{-1} at 253 K, which is about ten times faster than that in DMF solution with 0.4 mol l^{-1} Et_4NClO_4 as a supporting electrolyte. A significant contribution of solvent dielectric friction to the barrier crossing dynamics was shown in the DMF solution. In THF solution, much slower electron transfer rates were observed (8.0×10^8 s^{-1} at 253 K). This retardation was attributed to the slow relaxation time of the effective electric field by the neighbouring Na[cryptate]$^+$ cation.[82]

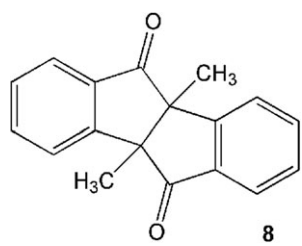

8

It has been demonstrated that spin-labelling may be used to monitor weak host–guest interactions, for example using the resorcinarene **9**, which bears four TEMPO units. Slow crystallisation of **9** from a mixture of CH_2Cl_2 and acetonitrile was found to produce crystals of sufficient quality for X-ray diffraction, revealing the presence of a single MeCN molecule disordered over two positions and contained within the cavity of **9**. X-Band EPR spectra of the complex were recorded at 295 K in non-viscous solvents, under which conditions it was expected that dipolar interactions would be averaged-out by rapid molecular tumbling. In $CHCl_3$ solution, a change in the lineshape occurs that is indicative of a weak exchange interaction between the spins, similar to that observed in the EPR spectra of nitroxides present in high concentration. The effects of exchange are further increased in 1 : 1 $CHCl_3$/MeCN. The average distances between the nitroxide groups in **9** are further decreased by the

presence of the guest in the cavity. Spectra of **9** were also recorded in the presence of other potential guest molecules such as $MeNO_2$, CH_2Cl_2 and EtOH, but MeCN remained unique in its ability to significantly modulate the EPR lineshape. Thus, the effects of exchange interactions between closely-spaced radicals could be used to monitor guest occupation in the host–guest complexes.[83]

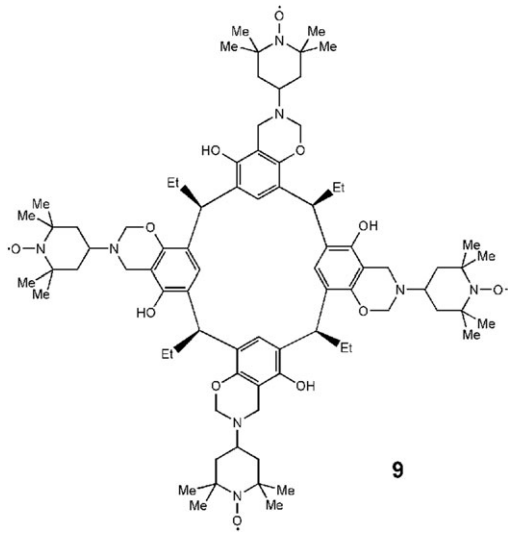

9

Conclusive proof has been demonstrated that the thermally-excited open-shell state with biradical character, **11**, contributes to the ground state of a formally closed shell molecule, namely the tetrafluoro derivative, **10**, of 1,4-bis((4,5-diphenylimidazo-2-ylidene)cyclohexa-2,5-diene. A small increase in the population of species **11** results in the formation of dimer **12**. The energy gap between states **10** and **11** is calculated to be 4.35 kcal mol^{-1}, which is appreciably smaller than the corresponding value for the parent 1,4-bis((4,5-diphenylimidazo)-2-ylidene)cyclohexa-2,5-diene molecule, which is calculated as being 7.54 kcal mol^{-1}. The presence of an enhanced 0.4% extent of contribution of biradical **12** to the solution, following light excitation, as compared to 0.1% for the non-fluorinated parent material, deduced from optical measurements, was confirmed by ESR.[84]

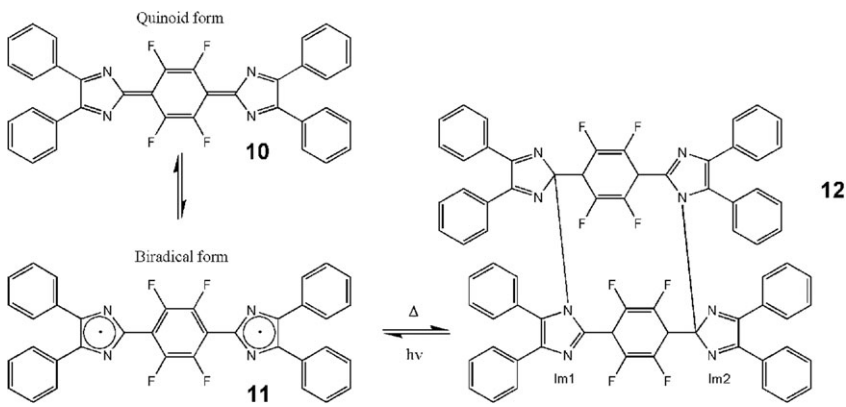

A set of compounds of type **13**, with two *para*-phenoxyl radicals bridged by a 1,2-diphenylenesilanylene unit in *meta*,*para* and *para*,*para* orientations, was synthesised, and the intramolecular spin–spin interaction investigated on the basis of Curie plots of ESR signal intensities from the "half-field" ($\Delta M_S = \pm 2$) transition at low temperature. When the bridging diphenylenesilanylene unit was arranged such that the two phenoxyl moieties were substituted respectively at a *meta* and a *para* position, this led to either a triplet ground state or to the degeneracy of the triplet and singlet states; in contrast, when both phenoxyl groups were *para*-substituted, a singlet ground state was observed instead.[85]

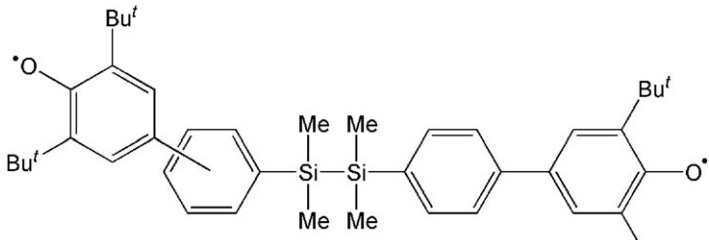

13

Stabilized radicals

Compound **14** has been synthesised, which may be considered as a paramagnetic derivative of DL-pipecolic acid, a homologue of proline. **14** was explored as a precursor to compounds of type **15**, where R = Boc, Tmpc, Fmoc or Nvoc (Boc = *tert*-butoxycarbonyl, Tmpc = 1-piperidinyloxy-4-carbonyloxyl-2,2,6,6-tetramethyl, Fmoc = 9-fluorenylmethyloxycarbonyl, Nvoc = 3,4-dimethoxy-6-nitrobenzylcarbamate). It is suggested that a novel paramagnetic hydroxytetramethylpiperidine protecting group might be introduced as a spin-label to follow the incorporation of an amino acid into peptides.[86] 2-(aminomethyl)-2,4,4-trimethyl-3-oxazolidinyloxyl hydrooxalate (**16**) was synthesised by a separate group of workers. **16** may be considered as a derivative of DOXYL (4,4,-dimethyl-3-oxazolidinyloxyl), and was synthesised by reacting 1-chloro-2-propanone with the potassium salt of 1*H*-isoindole-1,3-(2*H*)-dione to yield 2-(2-oxopropyl)-1*H*-isoindole-1,3(2*H*)-dione, which was then treated with 2-amino-2-methyl-1-propanol to give a 2-(phthalimidomethyl)-2,4,4-trimethyl-3-ozazolidinyloxyl radical, which, on deprotection, gave **16**. Since **16** is water soluble, it is a promising candidate for a variety of applications, and it may be further functionalised by reaction with *e.g.* ethyl chloroformate or chloroacetyl chloride, thus generating novel spin-labelling reagents.[87]

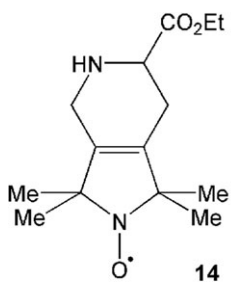

14

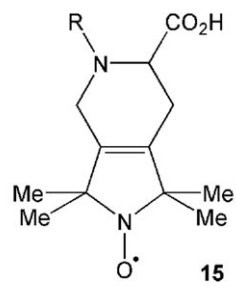

15

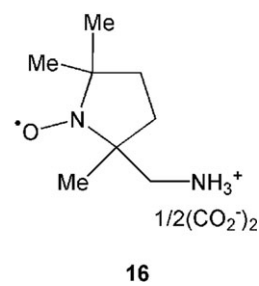

16

The reaction of 2-bromo-4,4,5,5-tetramethyl-4,5-dihydro-1*H*-imidazole-3-oxide-1-oxyl with sodium azolides, *e.g.* sodium 2-pyrazolide, yielded derivatives such as **17**. The C–N bond that joins the two rings is readily hydrolysed. Reduction of these compounds leads to corresponding derivatives, *e.g.* **18**, which are far more resistant towards hydrolysis. The structures of these compounds, confirmed by X-ray crystallography, showed that the paramagnetic molecules form packing arrangements with motifs ranging from centrosymmetric dimers to topologically-linear chains.[88]

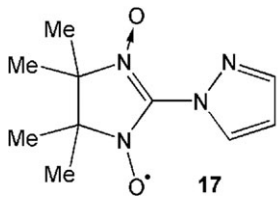

17

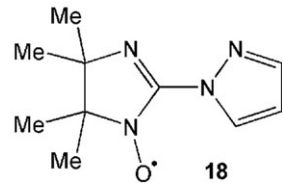

18

A most important paper has appeared, dealing with the origin of the enigmatic γ-splitting, observed in the ESR spectrum of the DMPO–OOH spin-adduct (A_N = 14.3 G, A_H^{β} = 11.7 G, A_H^{γ} = 1.25 G) when superoxide is trapped by DMPO. This radical is entirely characteristic of the DMPO–OH adduct (A14N = A1H = 14.9 G). The authors consider three possible explanations to account for the unique EPR spectrum of DMPO–OOH. The first is that the 1.25 G splitting arises from one of the H-atoms at either carbon 3 or carbon 4 of the DMPO–OOH ring. The second is that the splitting is from the unique H-atom of the OOH group. The third is that the conformational properties of the adducts change upon going from DMPO–OH to DMPO–OOH. A combined experimental and theoretical approach was used to find the correct explanation, and it was concluded that the above explanations were all wrong; the small splitting not coming from a hyperfine coupling but instead representing the presence of additional conformers of DMPO–OOH. Thus, the ''splitting'' is actually the result of the superposition of the spectra of two separate and individual conformers of DMPO–OOH.[89]

A cyclopentadienyl radical annelated with two homoadamantane frameworks, **19**, was synthesised and isolated in a stable crystalline form from single electron oxidation of the corresponding cyclopentadienyl anion **20**. The X-ray structure of **19** showed clearly a distinct bond alternation in the cyclopentadienyl ring, suggesting that the radical has the characteristics of a spin-localised 2,4-cyclopentadien-1-yl radical. The two homoadamantane frameworks are non-equivalent in crystals at 100 K, while ESR spectra indicate that they are equivalent when measured in a toluene solution at room temperature.[90] My own suggestion is that the authors are witnessing a Jahn–Teller distortion, similar to the type reported previously for the radical cations of benzene[91] and hexamethylbenzene.[92] Both the benzene radical cation and the cyclopentadienyl radical contain a delocalised system of five π-electrons, of which three are ascribed to a pair of ψ_A and ψ_S orbitals that are energetically degenerate. Thus the Jahn–Teller effect comes into play, and a structural distortion was observed at low temperatures for both the benzene radical cation and its hexamethyl derivative, both of which became dynamically averaged by increasing the temperature. Interestingly, the nature of the distortion was different in the two cases, with the ψ_S level becoming the SOMO (singly-occupied molecular orbital) in the parent benzene radical cation,[91] while a ψ_A SOMO was observed in the hexamethylbenzene radical cation.[92] DFT calculations on **19** give the following spin-density distribution: C1, 0.606; C2, −0.174; C3, 0.377; C4, 0.245; C5, −0.093,

which accords with an essentially ψ_S type SOMO, with the majority of the spin-density localised on a single carbon atom (C1), a node passing close to the C2 and C5 atoms (hence the negative spin-densities resulting from π–π electron spin-polarisation), and the remainder of the unpaired electron population located on C3 and C4. It is the presence of the *tert*-butyl group which causes an inequivalence of the C3 and C4 spin-densities. A simulated ESR spectrum, based on hyperfine coupling constants calculated for **19**, gave a poor agreement with that measured in a toluene solution at ambient temperature. However, when the simulation was undertaken in terms of a time-averaged structure between two equivalent distorted forms of **19**, the agreement was excellent. It was further calculated that the symmetrically-delocalised structure lay 2.57 kcal mol^{-1} higher in energy than the distorted structures of **19**, so providing a barrier sufficiently low that interconversion of the two isomers occurred rapidly enough that no line-broadening was observed, even when the temperature of the toluene solution was reduced to –130 °C.[90]

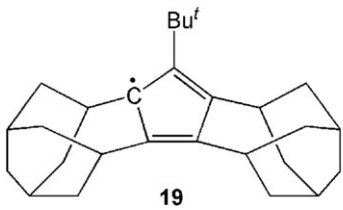

19

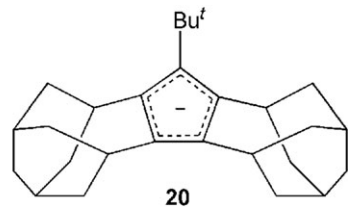

20

The compound [1,2,5]thiadiazolo[3,4-*c*][1,2,5]-thiadiazole (**21**) was synthesised in 62% yield by fluoride ion-induced condensation of 3,4-difluoro-1,2,5-thiadiazole with $(Me_3SiN:)_2S$. The radical anion of **21** could be formed reversibly by electrochemical reduction and further reduced to the dianion. The radical anion of **21** was characterised by ESR spectroscopy, both in solution and in the crystalline state. Stable salts were isolated for X-ray diffraction structural measurements.[93]

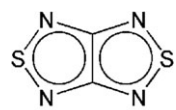

21

Cyclic voltammetry and ESR measurements were made on some poly (trifluoromethyl)fullerene derivatives, namely 1,9-$C_{60}(CF_3)_2$ and three isomers of $C_{60}(CF_3)_{10}$, including the structurally characterised derivative 1,3,7,10,14,17,23, 28,31,40-$C_{60}(CF_3)_{10}$, $C_{60}(CF_3)_{10}$. Compounds 1,9-$C_{60}(CF_3)_2$ and $C_{60}(CF_3)_{10}$ showed two reversible reductions, while the other two isomers showed only one. The ESR spectrum of the $C_{60}(CF_3)_{10}^{3-}$ radical anion consisted of an envelope of 25 lines centred at $g = 2.0032$, with an apparent splitting of 0.5 G, indicating coupling of the unpaired electron to a significant number of fluorine nuclei. Most significantly, this radical anion has a half-life in solution at 25 °C of around 7 min.[94] The highly twisted tetrakis(di-*tert*-butylmethylsilyl)disilene, $(Bu^t_2MeSi)_2Si{=}Si(SiMeBu^t_2)_2$, was prepared and reacted with Bu^tLi in THF to form its radical anion. The radical anion could be isolated as its lithium salt for X-ray analysis, which showed a nearly orthogonal geometry, with a twist angle of 88° between the two Si_2Si units, and with the central Si–Si bond elongated by 3.6% relative to the parent molecule. The interesting feature of this radical anion is that one of the central Si atoms has a

radical character while the other has anionic character, and an ESR study of the ^{29}Si coupling constants indicates that rapid spin-exchange occurs between these central Si atoms on the ESR timescale.[95] A density functional study has been reported of some rigid aliphatic semi-dione radical anions, *e.g.* bicyclo[2.2.1]heptane-2,3-dione. The calculated results are found to be in excellent agreement with the experimental results, as seems so often the case with DFT results (a long way forward from INDO, which I used when I first started working on radicals), but the authors also show that rather computationally cheaper theoretical methods also provide good agreement with experimental data.[96] Although the vinyl radical is certainly not stable and is highly reactive, I include it now as a fundamentally important organic radical. In one study, vinyl radical was produced in the gas phase in the ground vibronic state in a supersonic jet expansion by 193 nm excimer laser photolysis of vinyl bromide, and investigated using millimeter-wave spectroscopy. Due to proton tunnelling between the two equivalent ''bent'' forms of the molecule, the ground sate is split into two components. A set of precise molecular constants was obtained, including the proton tunnelling splitting in the ground state, determined as 16 272(2) MHz, and the potential barrier height from the proton tunnelling splitting, estimated to be 1580 cm^{-1}, by an analysis using a detailed one-dimensional model. The hyperfine interaction constants due to the α-proton and the two β-protons are consistent with the values measured from ESR studies of the vinyl radical.[97] Feldman's group in Moscow have used a combination of ESR and IR to study vinyl radicals formed by annealing rare gas matrices containing H-atoms and acetylene, in which the product vinyl radicals remain isolated. Two vibrational modes of the vinyl radical (ν_7 and ν_5) were assigned from the IR experiments, which were based on data for various isotopically (^{13}C, ^{2}H) substituted vinyl radicals, and confirmed by ESR and DFT calculations. The data on the ν_7 mode are in accord with previous experimental and theoretical results, however, the ν_5 frequency agrees well with the computational data but conflicts with gas phase IR emission results.[98] I conclude the organic radicals section with mention of a paper whose subject is highly relevant to current thinking about the world's future energy production, and indeed the future of life upon it, *i.e.* ''Methane Hydrate''.[99] Methane hydrate is formed when methane gas and water are brought together under suitable conditions of low temperature and elevated pressure, such that an ''ice'' type structure is formed containing methane molecules in considerable quantity. It is thought that vast quantities of methane hydrate exist on ocean beds, in the sediment of sea floors and in permafrosts, and some speculate that it might be possible to harvest the material to provide a massive reserve of methane as a fuel. On the negative side, it is known that drilling into methane hydrate poses a hazard to oil prospecting operations, and it is also thought that decomposition of methane hydrate by an eruption of methane could trigger a tsunami.

More catastrophically, it is believed by some that worldwide-scale eruptions of methane from these ''ice'' deposits have triggered climate change (global warming) on a cataclysmic level in the past, most notably the Permian–Triassic (P–T or PT) extinction event, sometimes informally called the Great Dying, that occurred approximately 252 million years ago, forming the boundary between the Permian and Triassic geologic periods. It was the Earth's most severe extinction event, with about 90 percent of all marine species and 70 percent of terrestrial vertebrate species becoming extinct.[100] For some time after the event, fungal species were the dominant form of terrestrial life. While I digress on this interesting topic, the paper referred-to reports a measurement of the decay of methyl radicals in methane hydrate, formed by exposure of the material to γ-rays.[99] It was found that the methyl radicals decay

by two different temperature-dependent processes. The activation energy for the lower temperature range (210–230 K) is 20.0 ± 1.6 kJ mol^{-1} and for the higher temperature range (235–260 K) is 54.8 ± 5.7 kJ mol^{-1}. The former value agrees well with the enthalpy change for methane hydrate dissociation into ice and methane gas, while the latter is in good accord with the enthalpy change for the dissociation into liquid water and gaseous methane. It is known that methane hydrates decompose into supercooled liquid water and gaseous methane at 235–260 K.

5. Materials

Nanomaterials

The existence of two temperatures: T_p—Cooper pairing and T_e—Bose–Einstein condensation in high temperature superconductors was stipulated in a lightly potassium metal-doped C_{60} by magnetically-modulated microwave absorption. The doping level corresponded to a carrier density greater than the critical one: $x > x_1$. When rubidium was used as the dopant, when the carrier density was less than the critical one: $x < x_1$, an anomalous temperature dependence of the ESR signal was noted. The characteristic temperature of bound electron pair formation ($T_p \approx 65$ K) and the energy gap ($2\Delta/k = 30$ K) were estimated from the temperature dependence of the ESR signal in a non-superconducting atate. The results suggest that the liquid fermions–liquid bosons transition can be observed by the opening of the spin gap at the temperature (T_p) postulated in Micnas–Ranninger–Robaszkiewicz theory.[101] There has been a report of two-temperature EPR measurements of macroscopic bundles of multi-walled carbon nanotubes, in which asymmetric resonance lines were observed. The contribution of localised π-electron spin centres was higher than in pyrolytic graphite. These results are interpreted in terms of an increase in the trapped electron density caused by the curvature of the nanotube graphene sheets.[102] Using pulsed-ESR methods, the basic spin relaxation behaviour of $N@C_{60}$-based peapods was elucidated. It was found that, in contrast to the narrow line spectra that are characteristic of $N@C_{60}$ in solid solution or in a C_{60} matrix, substantial line broadening is observed for the single-walled carbon nanotube (SWCNT)-encapsulated $N@C_{60}$ molecules, and that this might be indicative of a uniaxial cage distortion caused by interaction with the nanotube.[103] A high filling of SWCNTs with C_{60} and C_{70} fullerene molecules has been reported to occur at temperatures ≥ 69 °C. A two hour long reflux of a mixture of the fullerenes with SWCNTs in *n*-hexane resulted in a high yield of a C_{60},C_{70}@SWCNT peapod material. The peapod filling was determined by means of TEM, Raman, EELS and X-ray diffraction. Paramagnetic and temperature-sensitive ($N@C_{60,}C_{70}$)@SWCNTs were also prepared by this method, upon which ESR measurements were made. It was found that these solvent-prepared peapod samples can be transformed into double-walled carbon nanotubes (DWCNT) in sufficiently high yield that the process can be scaled-up.[104] Composites of cadmium selenide and indium phosphide nanoparticles with poly(2-methoxy-5-(3,7-dimethyloctyloxy)-1,4-phenylenevinylene) in different ratios were prepared. The quenching of the photoluminescence, the formation of polaronic radicals and the observation of two new conduction bands are explained in terms of a photoinduced charge transfer between the polymer and the nanocrystal. The charge transfer process was confirmed using ESR, and the *g*-factor of the polymer cation was measured. Time dependent studies show that long-lived polymer radicals are involved in the recombination process.[105] The ESR and other spectral properties of nanotube titanic acid, first dehydrated under

vacuum, were determined. After treatment under vacuum, single electron-trapped O-vacancies were detected by ESR, characterised by a symmetrical ESR signal with $g = 2.003$, the intensity of which grew according to the length of treatment. The O-vacancies played the role of F-centres, and the visible light absorption power of the material was found to be proportional to the ESR signal intensity. A possible mechanism for the formation of these centres in considered.[106] The generation of the superoxide radical anion by photosensitisation of TiO_2 nanoparticles with carotenoids on irradiation with red light has been demonstrated. At low concentrations of carotenoid ($<3 \times 10^{-5}$ M), the rate constant for $O_2^{\bullet -}$ production was found to exceed that measured in the absence of the carotenoid. Both superoxide and singlet oxygen are produced when the TiO_2 suspensions are irradiated in a toluene or CH_2Cl_2 solution, according to ESR experiments using respectively PBN and 2,3,6,6-tetramethylpiperidone. It is proposed that the dismutation of $O_2^{\bullet -}$ provides a source of singlet oxygen through the intermediate formation of $HO_2^{\bullet}$.[107]

EPR measurements have been employed in a study of colour centres in nanoporous glasses impregnated with copper β-diketonate by means of supercritical carbon dioxide. Along with optical absorption measurements, the results show that the Cu^{2+} ions are located in octahedral sites with D_{4h} coordination symmetry. The intensity of the EPR signal was found to decrease by an order of magnitude following an annealing of the glass at 200 °C, corresponding to the thermal decomposition of copper β-diketonate, to form metallic copper and CuO. This process is accompanied by a change in the form of the EPR spectrum and its corresponding spin Hamiltonian parameters, although the D_{4h} coordination symmetry is preserved. It is assumed that the remaining Cu^{2+} ions form new complexes with fragments of the decomposed ligands. It is concluded that high temperature annealing forms metallic copper nanoparticles within the glass.[108] It was found that two distinct ESR signals are recorded from nanocrystalline MgO formed by an aerogel method, and which are assigned to F^+-centres and $-O-CH_2^{\bullet}$ radicals formed from residual methoxide groups present at the points-of-contact between the nanocrystals. The F^+-centres were found to be stable up to 500 °C in an oxidising atmosphere, whereas the signal from $-O-CH_2^{\bullet}$ radicals could be removed by heating to 300 °C in the presence of oxygen. UV irradiation of the samples in the presence of oxygen resulted in the formation of 4-coordinated surface ($O-O_2^{\bullet -}$) radical anions; no signal from 3-coordinated radical anions was observed. The presence of strong Lewis acid and base sites on the surface of aerogel-prepared MgO was established using the adsorption of TEMPONE (2,2,6,6-tetramethyl-4-oxo-1-oxyl) and dinitrobenzene, respectively.[109] The temperature and frequency dependence of the magnetic properties of iron oxide nanoparticles were determined in the range 10–300 K using ESR. The linewidth of the signal was found to decrease slightly with decreasing temperature down to 100 K, and then to increase sharply down to 60 K; below 60 K, the trend is reversed, and the linewidth once again increases. The resonance field remains nearly constant down to 100 K, but then falls markedly as the temperature is decreased further. The resonance field for Fe_3O_4 showed a linear dependence on the microwave frequency. From the results, an effective g-value of 1.9846 and an internal field of −40 G were deduced.[110]

Catalysis

There is some overlap with the previous subsection, according to whether the focus of the article is on the ''nanomaterial'' or ''catalytic'' aspect of the particular sample;

hence some of the catalysts now considered are actually used in the form of nanoparticles. For example, the ternary oxide $(MoVW)_5O_{14}$ is an important material for performing mild, selective, catalytic oxidation reactions. By means of a combination of UV/visible, EPR and ^{95}Mo NMR, the coordination chemistry of the molybdate species in the precursor solutions was investigated. The results establish that mixing the precursor solutions (ammonium heptamolybdate, ammonium metatungstate and vanadyl oxalate) produces a polymeric network, in which the vanadyl species act as a linker between the molybdate units. The admixture of tungsten atoms is found to significantly augment the process of polymerisation.[111] TiO_2 nanotubes, with an average diameter of 15–20 nm and an active surface area greater by a factor of thirteen in comparison with TiO_2 powder, were synthesised by the reaction between TiO_2 particles and NaOH solution. When this nanotubular material was exposed to NO_2 gas, NO_2 molecules were strongly adsorbed onto the surface, from which an intense echo signal was detected from pulse-ESR experiments conducted below 200 K. A field-sweep-echo experiment revealed two distinct signals: three lines at $g = 2$ from the NO_2 radical, and a broad line with singularities at $g = 2.09$ and $g = 2.49$, whose origin is, as yet, unclear. Spin–lattice relaxation measurements showed that at temperatures above 50 K, the reorientational dynamics of adsorbed NO_2 molecules is thermally activated ($E_a = 10$ meV), while at lower temperatures than this, they become nearly static on the EPR timescale. Upon prolonged heating at 60 °C in air, the NO_2 signal was almost entirely lost.[112] A study has been reported of the paramagnetic defects in silicon nanowires produced by oxide-assisted growth, as detected by conventional X-band ESR spectroscopy. Three different kinds were identified: dangling bonds or P_b-centres with $g = 2.0065$, located at the interface between the crystal core and the surrounding oxide, E′-centres with $g = 2.0005$, and EX-centres with $g = 2.00252$, located in the oxide. For the EX-centres, a characteristic hyperfine splitting of 16.4 G was observed.[113] Silver atoms in molecular sieves continue to provide a topic for ESR investigations. For example, cationic silver clusters of differing nuclearity have been produced by radiolysis of Ag/H-SAPO-17 and Ag/H-SAPO-35, for which the ESR results show that the presence of absorbate molecules within the lattice is necessary to render them stable. In Ag/H-SAPO-17, cationic silver clusters trapped inside the cancrinite cages are stabilised by interactions with water or methanol molecules that are simultaneously present therein. ESEEM measurements were carried out in order to investigate the local structure of the silver dimers and trimers in the Ag/H-SAPO molecular sieve. It is proposed that the Ag_2^+ dimer, situated in a hexagonal prism, interacts with two H_2O molecules in two different levyne cages, whereas the Ag_3^{2+} trimer is located in the levyne cage close to a hexagonal prism, and is stabilised by interactions with four methanol molecules.[114] The interaction between silver atoms and ethylene in the Ag-SAPO-11 molecular sieve has also been studied under conditions of ionising radiation. It is thought that complexes such as $Ag(C_2H_4)_2$ can play a role as reactive intermediates in the catalytic conversion of ethylene by Ag-loaded molecular sieves. The ESR signal remained stable, even at 290 K. The hyperfine coupling constants calculated for the $Ag(C_2H_4)_2$ complex in D_{2h} symmetry using DFT are found to be in very good agreement with the experimental values.[115]

The interaction of NO with various types of iron-containing pentasilic zeolites was investigated using ESR. The systems studied were Fe-silicalite, ion-exchanged ZSM-5 and a bare silicalite impregnated with Fe ions on the surface only. It was found that NO reacts with Fe in all of these systems, which essentially functions as Fe^{2+}. Three distinct types of nitrosyl adduct were identified, all of which showed an absence of

hyperfine structure. Two of them are in doublet ($S = \frac{1}{2}$) states, while the third, observed only in the ZSM-5 samples, is a quadruplet ($S = \frac{3}{2}$) state. While all activated samples show similar spectra from Fe^{3+} ions, their reactivities towards NO are quite different. This permits some insight into the state of activated iron-containing pentasil type zeolites, which are of great importance in heterogeneous catalysis.[116] The ESR spectrum of a spin-probe in 2-propanol, condensed from the vapour phase into the nanochannel of MCM-41, showed three well-separated nitrogen hyperfine lines, indicating that the system exists in an essentially liquid phase in the channels, although the rotational diffusion of the probe is considerably restricted compared to a fluid solution. When a mixed solvent of 2-propanol and cyclohexane was employed, the ESR spectrum showed the presence of two components, indicating that the solution is phase-separated in the nanochannel. When all of the available space in the MCM-41 layer, including that among the granules, is filled with the solution, the absorbed molecules attain a yet higher mobility, and phase-separation is suppressed, even in the nanochannel.[117] In a related investigation, the molecular "packing" of long-chain *n*-alkanes in the MCM-41 nanochannel was examined. In this study, γ-irradiation at 77 K of the *n*-alkanes, *n*-decane, *n*-undecane, *n*-dodecane and *n*-tridecane, as sorbed into MCM-41, was observed to produce radicals that could be detected by ESR. It is noteworthy that the spectra recorded for these different alkanes were almost identical. Since the ESR spectra for the radiation-induced pure hydrocarbon crystals (which are due to three distinct kinds of radical: $^{\bullet}CH_2CH_2R$, $CH_3{}^{\bullet}CHCH_2R$ and $RCH_2{}^{\bullet}CHCH_2R$) change alternately as the number of carbon atoms varies consecutively, the results suggest that these alkanes are solidified in a similar way, and are therefore unable to form perfectly crystalline phases in the nanochannel. A model is proposed for the packing of the molecules, the relative yields of the three kinds of radicals do not deviate much from those for *n*-undecane and *n*-tridecane crystals.[118] The nature of the chemical bond between Cu^+ and NO in the gas phase, and in MFI (ZSM-5) and FER zeolites has been investigated using a combination of DFT and ESR methods. Theory shows that the magnitude of the isotropic hyperfine coupling to Cu nuclei is acutely dependent on the Cu–N═O bond angle, and values are obtained which are in good agreement with the experimental measurements. In the gas phase, the singly-occupied a′ orbital on NO interacts with the unoccupied 4s and 3g orbitals on Cu^+, which depopulates the antibonding SOMO and strengthens the N═O bond. In the copper–zeolite system, the electrostatic field increases the Pauli repulsion and pushes up the (occupied) 3d orbital energies so that they can interact with the a″ LUMO of NO. This interaction weakens the N═O bond. Two types of copper site were studied in the zeolite: on the channel wall and on the channel intersection. The interaction of NO with Cu^+ sites on the intersection is substantially stronger (29.5–27.1 kcal mol^{-1}) than with the Cu^+ sites on the channel wall (22.6–15.0 kcal mol^{-1}).[119] In another study, amine radical cations of type $R_4N^{\bullet+}$ and $R_3N^+CH_2{}^{\bullet}$ (where R = CH_3, C_2H_5, C_3H_7 and nitric oxide, NO) were used to probe the bonding to the surface, and the dynamics of radical species confined in the space of cages or channels in the zeolites, Al-offretite, SAPO-37, SAPO-42 and ALPO-5. The ESR spectra of $(CH_3)_3N^+CH_2{}^{\bullet}$ in various media were found to show temperature-dependent effects, indicative of a dynamic process. Free rotation about the $N–CH_2{}^{\bullet}$ bond was observed to occur in the temperature range 110–300 K, while the rotation of the methyl groups remained hindered. The tri-ethyl and tri-propyl derivatives were seen to undergo a different type of dynamic process, involving a two-jump process that interchanges the pair of methylene hydrogens. Pulsed ESR

was used to investigate NO–NO triplet state dimers formed in Na-A-type zeolite and their hyperfine interaction with Na^+ cations.[120] ESR has also been employed to monitor the photooxidation of guest molecules isolated in a self-assembled molecular cage, on the basis of the formation of a stable nitroxide radical under oxidising conditions.[121] Irradiation of 9,10-dicyanoanthracene or *para*-chloranil in the presence of *E*-1-benzylidene-2-phenylcyclopropane causes the latter material to undergo a methylenecyclopropane rearrangement. In contrast, when the material was incorporated into HZSM-5, the corresponding radical cation–zeolite complex was detected by ESR.[122] *In situ* ESR spectroscopy has been used to investigate different thermal- and light-induced processes that lead to the generation of superoxide radical anions on the surfaces of zirconia and sulfated zirconia materials. For both types of material, the *g*-values were found to be almost independent of the method of generation employed, and to depend on the nature of the surface state that stabilises the radical anions, so that the *g*-tensor anisotropy is significantly reduced on sulfated zirconia.[123] Evidence from ESR and UV/visible measurements has been reported that provides evidence for electron trapping at partially dehydrated MgO surfaces and shows that the presence of an isolated OH group on the surface drives the localisation of the excess electron onto exposed Mg^{2+} sites; when the number of OH groups is increased, the electron is instead delocalised over a number of OH groups.[124] From a combination of *in situ* Raman, XANES and EPR measurements, it is shown that in ceria-supported vanadium catalysts, the vanadium oxide species disperse with up to nine V atoms per nm^2 of support. Surface V^{5+} species interact closely with the ceria surface, thus promoting a reduction of Ce^{4+} to Ce^{3+}. Upon heating or during reaction, surface vanadia react with ceria to create a $CeVO_4$ phase. The catalytically-active site appears to be V^{5+}–O–Ce^{3+}.[125] The interaction of hydrogen peroxide with a range of polycrystalline TiO_2 systems, including TiO_2 powder, TS-1 (titanium silicalite), [Ti]-APO-5 and ion-exchanged Ti-ZSM-5, was investigated using X-band ESR spectroscopy. In all cases, the peroxide was immediately decomposed, with the formation of a variety of oxygen-centred radicals. In the TiO_2/H_2O_2 system, superoxide was produced, whereas in the TS-1/H_2O_2 medium, peroxyl type radicals were detected of the general form Ti–$OO^{\bullet}$.[126] The effects of additives on the photochemical production of hydroxyl radicals by TiO_2 was studied using the nitroxides 3-carboxy-2,2,5,5-tetramethyl-1-pyrrolidine-1-oxyl and 4-carboxyl-2,2,6,6-tetramethylpiperidine-1-oxyl. Of the additives investigated, only iodide ions were found to prohibit significantly the decay of the nitroxides, presumably by scavenging ''holes'' (electron vacancies) on the titanium dioxide surface.[127] A paper has been published on a study that clarifies the mechanism of the photocatalytic reduction of CO_2 by H_2 or CH_4 on a MgO surface. ESR showed that on the surface, CO_2 is reduced to the $CO_2^{\bullet-}$ upon photoillumination, and that this is reduced to a surface bidentate group by a dark reaction with the reductant hydrogen or methane.[128] The nature of electron traps at the surface of polycrystalline MgO was analysed for the first time by measurement of the ^{17}O couplings of the oxygen-centred anions present thereon by means of isotopically-enriched MgO. The trapped electrons were generated by exposure of the MgO samples to H_2, followed by UV irradiation, with the consequent production of proton/trapped electron centres (H^+)–e^-. The ESR spectrum shows a multiplet structure, with two sets of sextet features (with splittings of 51 G and 10 G) arising from two distinct and inequivalent ^{17}O nuclei.[129]

A rather unusual but highly interesting application of ESR has been reported that aims to understand the fundamental chemical processes that occur during the

pulverisation of quartz grains in geologically-active fault zones. Thus, quartz grains were crushed in pure water and the ESR spectra measured in order to quantify the silicon containing radicals thereby produced. It is shown that the H_2 gas formed arises *via* consumption of the Si-radical species.[130]

Two papers have been published on the topic of ESR investigations of operating processes involved in fuel cells. A miniature cell was constructed that can operate in the cavity of an EPR spectrometer, for monitoring *in situ* processes. It was shown possible to tune the cavity with the fuel cell running in it. An intense ESR signal was observed at $g = 2.0030$, which was thought to originate from the electrode material (0.00–2.00 mg cm^{-2} Pt on Vulcan XC-72 E-Tek). The behaviour of the signal is highly sensitive to the operating conditions; for example, when the cell was fed with oxygen, the signal intensity was found to decrease substantially, both under open- and closed-circuit conditions. This effect was noted for various different kinds of membrane.[131] A subsequent paper from this group is concerned with monitoring free radical formation and membrane degradation in a working fuel cell. By introducing a spin-trap at the cathode, the formation of immobilised radicals on the surface of Fluorine-free membranes thus revealed the onset of oxidative degradation. When a Nafion membrane was used, far less degradation was observed, and the hydroxyl radical was instead detected, suggesting that it is this species which causes the degradation of the fluorine-free membranes. At the anode, free radical intermediates of the fuel oxidation process were observed, and there was no evidence for membrane degradation on this side of the cell—which also supports the argument that the hydroxyl radical is the culprit for the membrane damage that is observed.[132] If we are to re-tool western society for the "hydrogen economy", so as to "burn" hydrogen in fuel cells, we will need to store hydrogen in great quantities, and I note one paper published on this general topic that reports ESR studies on the reactive Ti-containing radicals produced during the reversible hydrogenation of $NaAlH_4$ doped with Ti.[133] Many people are in favour of using "renewables" to provide for our energy needs in the future, but are probably not aware of the scale of change that would be required to accomplish the task.[134]

Polymers

I commence this section with a long-standing topic, that of radiation damage to polymers. This is a theme which runs throughout this section, and finds its significance in that radiation, in the form *e.g.* of electron beams, X-rays and γ-rays, is often used to process and surface-modify polymers, and to promote grafting operations. A good example is a study of the radiation chemistry of styrene/alkane and α-methylstyrene/alkane copolymers. The yields of radicals for the copolymers are as predicted, on the basis that the cross-section is proportional to the spin-density of each component, although there is some evidence for radical migration onto the aromatic groups at 77 K. Viscosity measurements were concluded to support a predominant cross-linking mechanism in the styrene/alkane copolymers, while in the α-methylstyrene/alkane copolymers, the main result of irradiation was found to be chain scission.[135] By means of a time-resolved ESR method, the excited triplet states of 1,6-(*N*-substituted)aza-[60]-1,2-(*N*-substituted)aziridino-[60]fullerene compounds were investigated, and evidence was presented for the involvement of intramolecular charge transfer states.[136] A review has been published of the use of ESR and ENDOR studies concerning the formation of solitons and polarons in polyacetylene and poly(*para*-phenylenevinylene) (PPV). High resolution ENDOR

spectra, obtained with stretch-oriented samples, yield the half-extension of 18 carbon atoms for CH_x and 4 phenyl rings in PPV.[137] By using a combination of ER and NMR, a study was made of conducting polymers intended for use in conjunction with biological materials such as artificial muscles. The radical scavenging properties of antioxidants consumed in the diet are often assessed by their ability to quench stable free radicals such as α,α-diphenyl-β-picrylhydrazyl (DPPH), and it was found that commercially available polyaniline and polypyrrole are efficient and rapid scavengers of DPPH, as monitored by ESR.[138] Two novel organic electron donors based on ethylthio-substituted tetrathiapentalenes, with a methylenedithio or a 1,3-dithiane unit, have been synthesised, and which form salts with a unique crystal structure that shows metallic conductivity down to low temperatures. The ESR line-shape is asymmetric.[139] ESR was used to study the structural anisotropy in several polythiophene derivatives. As the homogeneous width of the line was dominant, the spectra were Lorentzian in shape. Qualitatively, the extent of the anisotropy was in accord with that deduced previously from X-ray diffraction measurements, including a flip in molecular orientation with respect to the film substrate between the solution-cast and spin-cast films.[140] The synthesis of new 2,2,6,6-tetramethylpiperidin-1-oxyl (TEMPO) styryl derivatives for use as mediators in the living free radical polymerisation of styrene and *n*-butyl acrylate has been described. Two of the α-methyl groups at the 2- and 6-positions of the parent TEMPO styryl alkoxylamine were substituted by hydroxymethyl and silyloxymethyl groups. To further increase the steric hindrance around the alkoxylamine oxygen atom, the remaining two methyl groups were replaced by ethyl groups. As noted previously, it was found that intramolecular hydrogen-bonding led to a promotion of C–O bond homolysis, the kinetics for which were determined using ESR.[141] A review of the elementary steps involved in the initiation and termination processes of radical induced polymerisation has been published. Specifically considered are the kinetics of primary radicals produced by thermolysis or photolysis of RC(O)O–OR type peroxides and the correlation between the peroxide's structure and its rate of decomposition, and with initiator efficiency. It is shown that termination rate constants may be deduced as a function of temperature, pressure, polymer content and chain length using time-resolved IR to study monomer conversion or ESR to monitor the decay in radical concentration.[142] Another group has employed time-resolved EPR to study the addition of benzoyl radicals to *n*-butyl acrylate at both X-band (9 GHz) and W-band (95 GHz) frequencies. It is shown that the reactivity of the benzoyl radicals can be divided into two distinct domains: one is established at low concentrations (< 1.25 M) of *n*-butyl acrylate, with rate constants in the region of 10^6 mol^{-1} s^{-1}, while at higher concentrations of alkene, the rate is slowed by an order of magnitude, coinciding with the dramatic increase in viscosity of the medium.[143] A unique exponential attenuation-type oscillating curve was found when the photoinduced bulk polymerisation of a reactive hindered amine light stabiliser (4-acryloyl-2,2,6,6-tetramethylpiperidine) was carried out in air, but the phenomenon was absent when the process was performed under a nitrogen atmosphere. It is proposed that a recycling process occurs, in which nitroxide radicals are produced from the amine, as are detected by ESR.[144] ESR has been employed in a study of the photodegradation of syndiotactic and atactic polystyrene, from which it is concluded that the threshold wavelength for the formation of oxygenated products is 300 nm for both polymers.[145] The influence of block length (M_w = 12 000, 48 000 and 84 000) in polystyrene–block–polybutadiene copolymers on molecular dynamics was studied using spin-probes. Irrespective of which spin-probe was used (2,2,6,6-tetramethyl-4-

hydroxypiperidine-1-oxyl benzoate or 2,2,6,6-tetramethyl-4-hydroxypiperidine-1-oxyl), two spectral components were characterised according to a fast and a slower mobility, and which varied with the type of blocking unit.[146] The use of time-resolved ESR in studies of the photochemical degradation of acrylic polymers has been reviewed. It is shown that the method is mechanistically powerful, with a high spectral resolution and fast time response, and that experiments can be expanded by working at multiple frequencies and with several different sources of excitation.[147]

Solids

The temperature dependence of the low-field magnetoresistance in electron-doped manganites ($La_{1-x}Te_xMnO_3$) was determined over a range of temperatures between 5 and 300 K, for which a strong effect was observed when the temperature was far above the Curie temperature or when it was well below the metal–insulator transition temperature. Results from the ESR spectra and the magnetic field dependence of the resistivity suggested that the spin-polarised tunnelling between isolated ferromagnetic metallic clusters is probably responsible for the effect.[148] Interest in superconducting materials continues, though we remain somewhat distant from any wide scale practical replacement for conventional conductors that can function at room temperature. In one study, which employed a combination of optical and ESR, the oxidation states of cobalt ions in gehlenite ($Co:SrLaGa_3O_7$) were determined. Surprisingly, a Co^{2+} site is found to occupy octahedral sites within the structure, and the effect of UV irradiation was found to create colour centres in the lattice, which are attributed to Ga^{2+} centres.[149] The crystallographic phase, microstructure and dielectric properties of $BaTiO_3 + 0.02$ BaO and xCuO ceramics were studied: ESR spectra confirm that Cu^{2+} occupies Ti lattice sites, and that tetragonal and hexagonal phases coexist at room temperature for the material with $x \geq 0.003$ sintered in air at 1400 °C.[150] A very intriguing paper has been published which concerns the study, by ESR, of the insoluble organic matter in extraterrestrial and terrestrial rocks. The aim of the work was to distinguish between the biogenic and extraterrestrial origins of the organic matter found in meteorites, and it was discovered that a thermally excited triplet state existed in these materials due to biradical intermediates. Correlations of relaxation times and other ESR spectral properties with the age of the samples were established.[151] ESR dating methods were used to established the age of a population of tiny hominins in Indonesia, which are sufficiently distinct to be assigned to a new species: *Homo floresiensis*. It is concluded that they existed from before 38 000 years ago to 18 000 years ago.[152] The effect of high pressure, high temperature annealing on the paramagnetic defects in diamond was investigated by ESR.[153] The states of Fe^{3+} in various clay minerals, montmorillonites and layered double-hydroxides were studied by EPR.[154] ESR was also used to demonstrate that the average age of gypsum from the Lanzhou Basin was about 2.22×10^8 years.[155] Some new studies of ultramarine pigments were reported at both X-band and W-band frequencies, which enabled the resolution of the g-anisotropy of $S_3^{\bullet -}$ radicals, while W-band ENDOR provided evidence for strong coupling to Na^+ cations and a weaker interaction with ^{27}Al nuclei.[156]

6. Inorganic radicals

A new hole centre, Be^+, was detected by ESR with tetragonal symmetry in Be-doped MgO crystals.[157] The centre was destroyed above 160 K. The presence of hyperfine splitting from the ubiquitous Be impurity cations tended to complicate the form of

the ESR spectrum, and led, in fact, to a previous misinterpretation of the spectrum. A review has been published concerning the chemistry and EPR spectroscopy of Al, Ge and In cluster compounds, and the first direct detection of radicals using EPR in a Zeigler–Natta system.[158] Magnetic parameters were measured from the ESR spectra of the isotopomeric radicals: $Hg^{12}CH_3$, $Hg^{13}CCH_3$, $^{199}Hg^{12}CH_3$, $^{201}Hg^{12}CH_3$, $^{201}Hg^{13}CH_3$, $^{199}Hg^{12}CD_3$ and $^{201}Hg^{13}CH_3$, as isolated in an inert neon matrix.[159] High-field, multi-frequency EPR data have been obtained for the alum $CsMn(SO_4)_2 \cdot 12D_2O$, which are interpreted using the conventional $S = 2$ Hamiltonian to derive the corresponding zero-field and g-parameters.[160] An ESR study was made of a single crystal of the trimanganese cluster $Mn_3(O)(O_2CC_6F_5)_6(py)_3 \cdot CH_2Cl_2$. From the ESR analysis, it is shown that the ground state of this complex is $S = \frac{3}{2}$, based on the localised valence state model, in addition to the determination of the principal direction of the anisotropic hyperfine interaction. The result suggests that anti-ferromagnetic interactions between Mn^{3+} and Mn^{2+} ions are predominant.[161] The effects of ligands on the ESR and optical spectra of gold atoms formed from AuCl, initially dissolved in the liquid form of these compounds, in γ-irradiated solutions of the organic matrices solid 2-methyltetrahydrofuran and ethanol at 77 K, with and without HCl present, were examined. A remarkable dependence of the magnetic parameters on the polarity of the matrix was demonstrated. The ESR signals that were observed were the hyperfine quartet from transitions between the Zeeman levels of Au(0) atoms and a ground state nuclear spin $I = \frac{3}{2}$. Additionally, there were Au(0) atoms that showed a hyperfine interaction with magnetic nuclei from the matrix.[162] By means of ENDOR spectroscopy, the properties of Cu^{2+} and $(VO)^{2+}$ cations stabilised in polymers were investigated. It was found that the origin of the ENDOR signal is mainly due to anisotropic interactions between the unpaired spin and the nuclei of matrix atoms, such as water. A theoretical approach was used that seemed to work well, and its correctness was tested by comparing the temperature dependence of spin–lattice relaxation times, calculated from ENDOR line intensities, with the corresponding dependence obtained from stationary saturation ESR measurements. The activation processes of water self-diffusion and proton exchange are concluded to occur at higher temperatures, whereas it appears that a tunnelling mechanism is operative at reduced temperatures.[163] The spin Hamiltonian parameters of VO^{2+} ions incorporated into $GeO_2 \cdot Li_2O \cdot B_2O_3$ glasses were determined. It was found that there was no change in the tetragonality of the $V^{4+}O_6$ complex or in the size of the $3d_{xy}$ orbit with increasing GeO_2 content in the material.[164] The EPR spectra of the solid–liquid solution of manganese chloride in water under conditions of varying pressure have been reported. On the basis of a temperature jump change in the linewidth, the extent of supercooling of the solution was determined, depending on the pressure applied, at temperatures varying from 10 to 30 K. Such an extreme supercooling precludes ice-nucleation on the complex ions $Mn^{2+}(H_2O)_6$ and favours the formation of a eutectic structure shortly following the freezing of the solution.[165] Stable spirocyclic organometallic radicals, aluminium and gallium boraamidinates {[PhB(μ-NBu^t)$_2$]$_2$M$^\bullet$}, have been studied by ESR, following the oxidation of their corresponding lithiated anions with iodine. As supported by DFT calculations, the ESR spectra showed that the spin-density is symmetrically-delocalised over all four nitrogen atoms in these spiro-conjugated systems.[166] The structures and properties of bivalent nickel and copper complexes with pyrazine–amide–thioether coordination were investigated using ESR, demonstrating that a trivalent nickel species could be thus stabilised.[167] The electronic structures of arylalkynyl iron(III)

radical cations have been determined by ESR. It was observed that the principal hyperfine and *g*-values correlated with Hammett σ^+-constants in the complex series [Cp*Fe(dppe)(C$\equiv$CC$_6$H$_4$X-4)]PF$_6$.[168] Using time-resolved ESR, $HNO_2^{\bullet -}$ radicals were detected during the radiolysis of aqueous solutions of nitrite, formed by the addition of H-atoms to nitrite anions. The observed ^{14}N hyperfine splitting was 19.6 G, with a smaller splitting of 4.5 G from the unique proton and a *g*-factor of 2.0053. The results are consistent with those previously deduced from solid state studies.[169] The electrochemical reduction of sulfite ions in aqueous solution was found to occur by a two-electron reduction to SO_2, which was subsequently converted to the $SO_2^{\bullet -}$ radical anion.[170]

Acknowledgements

I thank my wife, Karen Blakeman, for providing invaluable technical support throughout the writing of this review.

References

1 C. J. Rhodes, *Annu. Rep. Prog. Chem., Sect. C: Phys. Chem.*, 2004, **100**, 149.
2 C. J. Rhodes, *Annu. Rep. Prog. Chem., Sect. C: Phys. Chem.*, 1999, **95**, 199.
3 H. Blok, J. A. J. M. Disselhorst, S. B. Orlinskii and J. Schmidt, *J. Magn. Reson.*, 2004, **166**(1), 92.
4 Y.-G. Zheng, F.-X. Dong, J. Xu, Y.-S. Xu, E. Shen, K. Wu, J.-B. Cong and D.-R. Zhang, *Bopuxue Zazhi*, 2003, **20**(3), 231.
5 F. Simon and F. Muranyi, Los Alamos National Laboratory, Preprint Archive, Condensed Matter, 2 September 2004, 1, arXiv:cond-mat/0409051. URL: http://xxx.lanl.gov/pdf/cond-mat/0409051.
6 G. Annino, M. Cassettari, M. Martinelli and P. J. M. van Bentum, *Appl. Magn. Reson.*, 2003, **24**(2), 157.
7 B. Epel, D. Arieli, D. Baute and D. Goldfarb, *J. Magn. Reson.*, 2003, **164**(1), 78.
8 G. L. Della, M. Pezzato, M. C. Baratto, R. Pogni and R. Basosi, *J. Magn. Reson.*, 2003, **164**(1), 71.
9 B. L. Bales, M. Peric and I. Dragutan, *J. Phys. Chem. A*, 2003, **107**(43), 9086.
10 B. L. Bales, M. Peric and I. Dragutan, *J. Phys. Chem. A*, 2002, **106**, 4846.
11 K. Fukui, T. Ito, M. Tada, M. Aoyama, S. Sato, J. Onodera and H. Ohya, *J. Magn. Reson.*, 2003, **163**(1), 174.
12 V. A. Livshita and D. Marsh, *J. Magn. Reson.*, 2005, **175**(2), 317.
13 S. K. Misra, *Appl. Magn. Reson.*, 2003, **24**(2), 127.
14 G. Gualtieri, S. Colacicchi, V. Carnicelli and A. Di Giulio, *Biophys. Chem.*, 2005, **114**(2–3), 149.
15 P. P. Borbat, J. H. Davis, S. E. Butcher and J. H. Freed, *J. Am. Chem. Soc.*, 2004, **126**(25), 7746.
16 G. Jeschke, A. Bender, H. Paulsen, H. Zimmermann and A. Godt, *J. Magn. Reson.*, 2004, **169**(1), 1.
17 V. A. Bagryansky, V. I. Borovkov and Y. I. Molin, *Phys. Chem. Chem. Phys.*, 2004, **6**(5), 924.
18 V. A. Livshits, B. G. Dzikovski and D. Marsh, *J. Magn. Reson.*, 2003, **162**(2), 429.
19 M. Bonora, S. Pornsuwan and S. Saxene, *J. Phys. Chem. B*, 2004, **108**(13), 4196.
20 N. J. Malmberg and J. J. Falke, *Annu. Rev. Biophys. Biomol. Struct.*, 2005, **34**, 71.
21 J. Kang, S. Tokdemir, J. Shao and W. H. Nelson, *J. Magn. Reson.*, 2003, **165**(1), 128.
22 F. J. Adrian, *J. Phys. Chem. A*, 2003, **107**(43), 9045.
23 R. Owenius, G. E. Terry, M. J. Williams, S. S. Eaton and G. R. Eaton, *J. Phys. Chem. B*, 2004, **108**(27), 9475.
24 V. A. Livshits, D. Kurad and D. Marsh, *J. Phys. Chem. B*, 2004, **108**(27), 9403.
25 J. Tamuliene, A. Tamulis and J. Kulys, *Nonlinear Anal.*, 2004, **9**(2), 185.
26 H. Dong and S. Wu, *Sichuan Daxue Xeubao, Ziran Kexueban*, 2002, **39**(5), 865.
27 F. A. Villamene, C. M. Hadad and J. L. Zweier, *J. Am. Chem. Soc.*, 2004, **126**(6), 1816.
28 R. R. Mett and J. S. Hyde, *J. Magn. Reson.*, 2003, **165**(1), 137.
29 J. W. Sidabras, R. R. Mett and J. S. Hyde, *J. Magn. Reson.*, 2005, **172**(2), 333.

30 A. Hirayama, S. Nagase, A. Ueda, K. Yoh, T. Oteki, M. Obara, K. Takeda, Y. Shimozawa, K. Aoyagi and A. Koyama, *Mol. Cell. Biochem.*, 2003, **244**(1–2), 63.
31 M. Paolini, L. Valgimigli, E. Marchesi, S. Trespidi and G. F. Pedulli, *Free Radical Res.*, 2003, **37**(5), 503.
32 H. Shoji, H. Miyazaki, F. Yoshino, Y. Omori, S. Takahashi, K. Todoki and M. Lee, *Shika Yakubutsu Ryoho*, 2003, **22**(1), 18.
33 S. K. Jackson, M. P. Thomas, S. Smith, M. Madhani, S. C. Rogers and P. E. James, *Faraday Discuss.*, 2004, **126**, 103.
34 Z. H. Taha, *Talanta*, 2003, **61**(1), 3.
35 T. Ozawa, *Farumashia*, 2004, **40**(4), 301.
36 M. P. Thomas, S. K. Jackson and P. E. James, *Adv. Exp. Med. Biol.*, 2003, **510**, 205.
37 M. Wrona, W. Korytowski, M. Rozanowska, T. Sarna and G. T. Truscott, *Free Radical Biol. Med.*, 2003, **35**(10), 1319.
38 T. Tokunaga, S. R. M. D. Morshed, S. Otsuki, F. Takayama, T. Satoh, K. Hashimoto, T. Yasui, S. Ogawa, H. Kanegae, Y. Yokote, K. Akahane, M. Kashimata, K. Satoh and H. Sakagami, *Anticancer Res.*, 2003, **23**(5A), 3719.
39 M. R. Bukowsi, S. Zhu, K. D. Koehntop, W. W. Brennessel and L. Que, *JBIC, J. Biol. Inorg. Chem.*, 2004, **9**(1), 39.
40 Y. Zhang and E. Oldfield, *J. Am. Chem. Soc.*, 2004, **126**(14), 4470.
41 R. Piskorski and J. Bernhard, *J. Am. Chem. Soc.*, 2003, **125**(43), 13120.
42 N. Pilton and W. Joachim, *Nucleosides Nucleotides Nucleic Acids*, 2003, **22**(5–8), 1664.
43 D. Flemming, A. Schlitt, V. Spehr, T. Bischof and T. Friedrich, *J. Biol. Chem.*, 2003, **278**(48), 47602.
44 Alia, B. Hulsebosch, H. J. van Gorkom, J. Raap, J. Lugtenburg, J. Matysik, H. J. B. de Groot and P. Gast, *Chem. Phys.*, 2003, **294**(3), 459.
45 M. R. Fuchs, A. Schnegg, M. Plato, C. Schulz, F. Muh, W. Lubitz and K. Mobius, *Chem. Phys.*, 2003, **294**(3), 371.
46 P. Pospisil, A. Arato, A. Krieger-Liszkay and A. W. Rutherford, *Biochemistry*, 2004, **43**(21), 6783.
47 N. Singh, K. K. Shukla, R. N. Patel, U. K. Chauhan and R. Shrivastava, *Spectrochim. Acta, Part A*, 2003, **59**(13), 3111.
48 K. Sakano, M. Mizutani, M. Murata, S. Oikawa, Y. Hiraku and S. Kawanishi, *Free Radical Biol. Med.*, 2005, **39**(8), 1041.
49 Z. Cai and M. D. Sevilla, *Top. Curr. Chem.*, 2004, **237**, 403.
50 E. Malinen and E. Sagstuen, *Radiat. Res.*, 2003, **160**(2), 186.
51 K. Stadler, M. Sasvari, J. Jakus, K. J. Jung, H. Y. Chung, I. Berkes, C. Nyakas and Z. Radak, *Brain Res. Bull.*, 2005, **65**(6), 487.
52 A. V. Chekanov, O. M. Panasenko, A. N. Osipov, N. S. Matveeva, K. D. Kazarinov, Yu. A. Vladimirov and V. I. Sergienko, *Biofizika*, 2005, **50**(1), 13.
53 T. L. Poulos, *Philos. Trans. R. Soc. London, Ser. A*, 2005, **363**, 1829–793.
54 D. Harris, in *Toxicology Of The Human Environment—The Critical Role Of Free Radicals*, ed. C. J. Rhodes, Taylor and Francis, London, 2000, pp. 397.
55 W. O. Feikema, P. Gast, I. B. Klenina and I. I. Proskuryakov, *Biochim. Biophys. Acta*, 2005, **1709**(2), 105.
56 S. H. Kim, W. Gregor, J. M. Peloquin, M. Brynda and R. D. Britt, *J. Am. Chem. Soc.*, 2004, **126**(23), 7228.
57 H.-D. Yu, R. Fang, S.-M. Chan and G.-L. Zou, *Huaxue Xuebao*, 2005, **63**(14), 1357.
58 T. Seino, A. Yoshioka, M. Takai and M. Tabata, *J. Appl. Polym. Sci.*, 2004, **93**(5), 2136.
59 M. Salem, K. Narendra, A. P. Brown and J. B. Wooten, *Prepr. Symp.–Am. Chem. Soc., Div. Fuel Chem.*, 2005, **50**(1), 419.
60 R. P. de Carvalho, J. R. Freitas, A.-M. G. de Souss, R. L. Moreira, M. V. B. Oinheiro and K. Krambrock, *Hydrometallurgy*, 2003, **71**(1–2), 277.
61 K. J. Reszka, P. Bilski and C. F. Chignell, *Nitric Oxide*, 2004, **10**(2), 53.
62 C. Rizzi, A. Samouilov, V. K. Kutala, N. L. Parinandi, J. L. Zweier and P. Kuppusamy, *Free Radical Biol. Med.*, 2003, **35**(12), 1608.
63 V. K. Kutala, N. L. Parinandi, J. L. Zweier and P. Kuppusamy, *Arch. Biochem. Biophys.*, 2004, **424**(1), 81.
64 K. Stolze, N. Udilova, T. Rosenau, A. Hofinger and H. Nohl, *Biochem. Pharmacol.*, 2003, **66**(9), 1717.
65 C. J. Rhodes, T. T. Tran and H. Morris, *Spectrochim. Acta, Part A*, 2004, **60**(6), 1401.
66 Y. Ohashi, Y. Takeuchi, M. Hirama, H. Yoshioka and H. Yoshioka, *Bull. Chem. Soc. Jpn.*, 2005, **78**(10), 1757.

67 D. A. Pratt, J. A. Blake, P. Mulder, J. C. Walton, H.-G. Korth and K. U. Ingold, *J. Am. Chem. Soc*., 2004, **126**(34), 10667.
68 P. Brandi, C. Galli and P. Gentili, *J. Org. Chem*., 2005, **70**(23), 9521.
69 W. Adam and C. M. O. Schulte, *Eur. J. Org. Chem*., 20047), 1482.
70 I. Nakanishi, K. Ohkubo, K. Miyazaki, W. Hakamata, S. Urano, T. Ozawa, H. Okuda, S. Fukuzami, N. Ikota and K. Fukuhara, *Chem. Res. Toxicol*., 2004, **17**(1), 26.
71 S. M. Khopde, K. I. Priyadarsini, M. K. Bhide, M. D. Sastry and T. Mukherjee, *Res. Chem. Intermed*., 2003, **29**(5), 495.
72 H. Karoui, J.-L. Clement, A. Rockenbauer, D. Siri and P. Tordo, *Tetrahedron Lett*., 2004, **45**(1), 149.
73 M. Mitsui, Y. Kobori, A. Kawai and K. Obi, *J. Phys. Chem. A*, 2004, **108**(4), 524.
74 M. Mitsui, K. Takeda, Y. Kobori, A. Kawai and K. Obi, *J. Phys. Chem. A*, 2004, **108**(7), 1120.
75 Z.-Y. Bian, X.-Q. Guo, Y.-B. Zhao and J.-O. Du, *Anal. Sci*., 2005, **21**(5), 553.
76 P. Tsai, J. M. Marra, S. Pou, M. K. Bowman and G. M. Rosen, *J. Org. Chem*., 2005, **70**(18), 7093.
77 L. Benisvy, R. Bittl, E. Bothe, C. D. Garner, J. McMaster, S. Ross, C. Teutloff and F. Neese, *Angew. Chem., Int. Ed*., 2005, **44**(33), 5314.
78 T. Sato, A. Narazaki, Y. Kawaguchi, H. Niino, G. Bucher, D. Grote, J. J. Wolff, H. H. Wenk and W. Sander, *J. Am. Chem. Soc*., 2004, **126**(25), 7846.
79 K. K. Mthilal, J. I. Johnson, R. Gandhidasan and R. Murugesan, *J. Photochem. Photobiol., A*, 2004, **162**(1), 9.
80 T. Ichino and R. W. Fessenden, *J. Phys. Chem. A*, 2003, **107**(44), 9257.
81 N. S. Nudelman, S. Velurtas and M. A. Grela, *J. Phys. Org. Chem*., 2003, **16**(10), 669.
82 H. Hosoi and Y. Masuda, *J. Mol. Liq*., 2005, **119**(1–3), 89.
83 L. Kroeck, A. Shivanyuk, D. B. Goodin and J. Rebek, Jr, *Chem. Commun*., 2004, **3**, 272.
84 A. Kikuchi, F. Iwahori and J. Abe, *J. Am. Chem. Soc*., 2004, **126**(21), 6526.
85 T. Iida, J. Ohshita, N. Ohta, K. Komaguchi, Y. Itagaki, M. Shiotani and A. Kunai, *J. Organomet. Chem*., 2003, **688**(1–2), 192.
86 M. Balog, T. Kalai, J. Jeko, Z. Berente, H.-J. Steinhoff, M. Engelhard and K. Hideg, *Tetrahedron Lett*., 2003, **44**(51), 9213.
87 J. R. Harjani, S. J. Nara, P. U. Naik and M. M. Salunkhe, *Tetrahedron Lett*., 2004, **45**(1), 179.
88 E. V. Tretyakov, G. V. Romanenko and V. I. Ovcharenko, *Tetrahedron*, 2004, **60**(1), 99.
89 G. M. Rosen, A. Beselman, P. Tsai, S. Pou, C. Mailer, K. Ichikawa, B.H. Robinson, R. Nielsen, H. J. Halpern and A. D. MacKerell, Jr, *J. Org. Chem*., 2004, **69**(4), 1321.
90 T. Kitagawa, K. Ogawa and K. Komatsu, *J. Am. Chem. Soc*., 2004, **126**(32), 9930.
91 M. Iwasaki, K. Toriyama and N. Nunome, *J. Chem. Soc., Chem. Commun*., 1983, 320.
92 C. J. Rhodes, *J. Chem. Soc., Chem. Commun*., 1989, 327.
93 A. Y. Makarov, I. G. Irtegova, Y. V. Gatolov, E. Lork, R. Mews and W.-D. Stohrer, *Inorg. Chem*., 2005, **44**(20), 7194.
94 A. A. Popov, J. Tarabek, I. E. Kareev, S. F. Lebedkin, S. H. Strauss, O. V. Boltalina and L. Dunsch, *J. Phys. Chem. A*, 2005, **109**(43), 9709.
95 A. Sekiguchi, S. Inoue, M. Ichinobe and Y. Arai, *J. Am. Chem. Soc*., 2004, **126**(31), 9626.
96 S. Ralhan, P. K. Shukla and N. K. Ray, *Indian J. Chem., Sect. A: Inorg., Bio-inorg., Phys., Theor. Anal. Chem*., 2003, **42**(10), 2493.
97 K. Tanaka, M. Toshimitsu, K. Harada and T. Tanaka, *J. Chem. Phys*., 2004, **120**(8), 3604.
98 H. Tanskanen, L. Khriachtchev, M. Rasanen, V. I. Feldman, F. F. Sukhof, A. Y. Orlov and D. A. Tyurin, *J. Chem. Phys*., 2005, **123**(6), 064318/1.
99 K. Takeya, K. Nango, T. Sugahara, K. Ohgakia and A. Tani, *J. Phys. Chem. A*, 2005, **109**(44), 21086.
100 http://en.wikipedia.org/wiki/Permian-Triassic_extinction_event.
101 J. Stankowski, L. Oiekara-Sady and W. Kemplinski, *J. Phys. Chem. Solids*, 2004, **65**(2–3), 321.
102 P. Szroeder, F. Rozploch and W. Marciniak, *Diffus. Defect Data, Pt. B*, 2003, **94**, 275.
103 A. Gembus, F. Simon, A. Janossy, H. Kuzmany and K. P. Dinse, *AIP Conf. Proc*., 2004, **723**, 259.
104 F. Simon, H. Kuzmany, H. Rauf, T. Pichler, J. Bernardi, H. Peterlik, L. Korecz, F. Fulop and A. Janossy, Los Alamos National Laboratory, Preprint Archive, Condensed Matter, 7 October 2003, 1–5, arXiv:cond-mat/0310110. URL http://xxx.lanl.gov/PS_cache/cond-mat/pdf/0310/0310110.pdf.

105 M. Pientka, J. Wisch, S. Boger, J. Parisi, V. Dyakonov, A. Rogach, D. Talapin and H. Weller, *Thin Solid Films*, 2004, **451–452**, 48.
106 S. Zhang, W. Li, Z. Jin, J. Yang, J. Zhang, Z. Du and Z. Zhang, *J. Solid State Chem.*, 2004, **177**(4–5), 1365.
107 T. A. Konovalova, J. Lawrence and L. D. Kispert, *J. Photochem. Photobiol., A*, 2004, **162**(1), 1.
108 V. N. Bagratashvili, L. D. Bogomolova, V. A. Jachkin, N. A. Krasil'nikova, A. O. Rybaltovskii, S. I. Tsypina and E. A. Chutko, *Glass Phys. Chem.*, 2004, **30**(6), 500.
109 R. M. Richards, A. M. Volodin, A. F. Bedilo and K. J. Klabunde, *Phys. Chem. Chem. Phys.*, 2003, **5**(19), 4299.
110 Y. Koeseoglu and B. Aktas, *Phys. Status Solidi C*, 2004, **1**(12), 3516.
111 S. Knobl, G. A. Zenkovets, G. N. Kryukova, R. I. Maksimovskaya, T. V. Larina, N. T. Vasenin, V. F. Anufrienko, D. Niemeyer and R. Schloegl, *Phys. Chem. Chem. Phys.*, 2003, **5**(23), 5343.
112 P. Cevc, P. Umek, R. Blinc, A. Jesih, B. Jancar and D. Arcon, *AIP Conf. Proc.*, 2004, **723**, 302.
113 A. Baumer, M. Stutzmann, M. S. Brandt, F. C. K. Au and S. T. Lee, *Appl. Phys. Lett.*, 2004, **85**(6), 943.
114 J. Michalik, J. Sadlo, A. Prakash and L. Kevan, *Stud. Surf. Sci. Catal.*, 2004, **154**, 1568.
115 M. Danilczuk, D. Pogocki, A. Lund and J. Michalik, *Phys. Chem. Chem. Phys.*, 2004, **6**(6), 1165.
116 P. Fisicaro, E. Giamello, G. Berlier and C. Lamberti, *Res. Chem. Intermed.*, 2003 **29**(7–9), 805.
117 M. Okazaki, K. Toriyama, N. Sawaguchi and K. Oda, *Bull. Chem. Soc. Jpn.*, 2004, **77**(1), 87.
118 K. Toriyama and M. Okazaki, *J. Phys. Chem. B*, 2004, **108**(34), 12917.
119 M. Davidova, D. Nachtgallova, P. Nachtigall and J. Sauer, *J. Phys. Chem. B*, 2004, **108**(34), 13674.
120 W. Liu, A. Lund, M. Shiotani, L. Michalik, D. Biglino and M. Bonora, *Appl. Magn. Reson.*, 2003, **24**(3–4), 285.
121 M. Yoshizawa, S. Miyagi, M. Kawano, K. Ishiguro and M. Fujita, *J. Am. Chem. Soc.*, 2004, **126**(30), 9172.
122 H. Ikeda, T. Nomura, K. Akiyama, M. Oshima and H. D. Roth, *J. Am. Chem. Soc.*, 2005, **127**(41), 14497.
123 A. F. Bedilo, M. A. Plotnikov, N. V. Mezentseva, A. M. Volodin, G. M. Zhidomirov, M. Ilya and K. J. Klabunde, *Phys. Chem. Chem. Phys.*, 2005, **7**(16), 3059.
124 M. Chiesa, M. C. Paganini and E. Giamello, *ChemPhysChem*, 2004, **5**(12), 1897.
125 M. V. Martinez-Heurta, J. M. Coronado, M. Fernandez-Garcia, A. Iglesias-Juez, G. Dea, J. L. G. Fierro and M. A. Banares, *J. Catal.*, 2004, **225**(1), 240.
126 K. L. Antcliffe, D. M. Murphy, E. Griffiths and E. Giamello, *Phys. Chem. Chem. Phys.*, 2003, **5**(19), 4306.
127 Y. Nosaka, S. Komori, K. Yawata, T. Hirakawa and A. Y. Nosaka, *Phys. Chem. Chem. Phys.*, 2003, **5**(20), 4731.
128 K. Teramura, T. Tanaka, H. Ishikawa, Y. Kohno and T. Funabiki, *J. Phys. Chem. B*, 2004, **108**(1), 346.
129 M. Chiesa, P. Martino, E. Giamello, C. Di Valentine, A. Del Vitto and G. Pacchioni, *J. Phys. Chem. B*, 2004, **108**(31), 11529.
130 K. Saruwatari, J. Kameda and H. Tanaka, *Phys. Chem. Miner.*, 2004, **31**(3), 176.
131 A. Panchenko, H. Dilger, E. Moller, T. Sixt and E. Roduner, *J. Power Sources*, 2004, **127**(1–2), 325.
132 A. Panchenko, H. Dilger, J. Kerres, M. Hein, A. Ulrich, T. Kaz and E. Roduner, *Phys. Chem. Chem. Phys.*, 2004, **6**(11), 2891.
133 C. M. Jensen, S. S. Srinivasan, R. Cantelli, O. Palumbo, A. Paolone, C. M. Andrei, H. W. Brinks, R. Holmstad, J. C. Walmsley, B. C. Haubeck, H. W. Brinks, M. Kuba, S. Eaton, D. Sun, K. Murphy and P. Wang, *Prepr. Symp.–Am. Chem. Soc., Div. Fuel Chem.*, 2005, **50**(2), 503.
134 http://ergobalance.blogspot.com.
135 F. Cardona, D. J. T. Hill, P. J. Pomery and A. K. Whittaker, *Polym. Int.*, 2003, **52**(11), 1711.
136 S. Yamauchi, Y. Iwasaki, Y. Ohba, B. Z. S. Awen and A. Ouchi, *Chem. Phys. Lett.*, 2005, **411**(1–3), 203.
137 S.-I. Kuroda, *Trans. Mater. Res. Soc. Jpn.*, 2004, **29**(3), 965.

138 P. A. Kilmartin, M. Gizdavic-Nikolaidis, Z. Zujovic, J. Travas-Sejdic, G. A. Bowmaker and R. P. Cooney, *Synth. Met*., 2005, **15391–3**, 153.
139 Y. Bando, T. Matsuzawa, N. Takashita, T. Kawamoto, T. Mori and J. Yamada, *Bull. Chem. Soc. Jpn*., 2005, **78**(8), 1442.
140 D. W. Breiby, S. Sato, E. J. Samuelsen and K. Mizoguchi, *J. Polym. Sci., Part B: Polym. Phys*., 2003, **41**(23), 3011.
141 C. A. Knoop and A. Studer, *J. Am. Chem. Soc*., 2003, **125**(52), 16327.
142 M. Buback, *Macromol. Symp*., 2005, 226–121.
143 D. Hristova, I. Gatlik, G. Rist, K. Dietliker, J.-P. Wolf, J.-L. Birbaum, A. Savitsky, K. Mobius and G. Gescheidt, *Macromolecules*, 2005, **38**(18), 7714.
144 X. X. Liu, X. H. Zhang, G. G. Wu, J. W. Yang, Z. H. Zeng and Y. L. Chen, *Chin. Chem. Lett*., 2003, **14**(10), 1085.
145 A. Torikai and H. Shibata, *Arabian J. Sci. Eng., Sect. C*, 2002, **27**(1), 11.
146 J. Culin, M. Andreis, Z. Veksli and Y. Gallot, *Polymer*, 2003, **44**(26), 7875.
147 M. D. E. Forbes, V. P. McCaffrey and E. J. Harbron, *Spectrum*, 2005, **18**(2), 12.
148 G. Ten, P. Duan, G. Yang, S. Dai, B. Cheng, Y. Zhou, H. Lu and Z. Chen, *J. Phys.: Condens. Matter*, 2004, **16**(8), 1447.
149 S. M. Kaczmarek and G. Boulon, *Opt. Mater*., 2003, **24**(1/2), 151.
150 H. T. Langhammer, T. Muller, R. Bottcher, V. Mueller and H.-P. Abicht, *J. Eur. Ceram. Soc*., 2004, **24**(6), 1489.
151 D. Gourier, L. Binet, A. Scrzypczak, S. Derenne and F. Robert, *Spectrochim. Acta, Part A*, 2004, **60**(6), 1349.
152 M. J. Morwood, R. P. Soejono, R. G. Roberts, T. Sutikna, C. S. M. Turney, K. E. Westway, W. J. Rink, J.-X. Zhao, G. D. van den Bergh, R. Awe Due, D. R. Hobbs, M. W. Moore, M. I. Bord and L. K. Fifield, *Nature*, 2004, **431**(7012), 1087.
153 R. N. Pereira, W. Gehlhoff, A. J. Neves, N. A. Sobolev, L. Rino and H. Kanda, *J. Phys.: Condens. Matter*, 2003, **15**(39), S2941.
154 F. Dijoux, B. Deroide and D. Tichit, 2001 A Clay Odyssey, in *Proc. Int. Clay Conf*., Bahia Blanca, Argentina, July 22–28, 2001 (pub. 2003), pp. 419, ed. E. A. Dominguez, G. R. Mas and F. Cravero, Elsevier Science B.V., Amsterdam.
155 S. Diao, Y. Ye, W. Sui and X. Li, *Diqiu Xuebao*, 2004, **25**(2), 209.
156 D. Arieli, D. E. W. Vaughan and D. Goldfarb, *J. Am. Chem. Soc*., 2004, **126**(18), 5776.
157 S. A. Diogov, V. Isakhanyan, T. Kaerner, A. Maaroos and S. Nakonechnyi, *J. Phys.: Condens. Matter*, 2003, **15**(40), 6871.
158 J. P. Maher, *Annu. Rep. Prog. Chem., Sect. A: Inorg. Chem*., 2003, **99**, 43.
159 E. Karakyriakos and A. J. McKinley, *J. Phys. Chem. A*, 2004, **108**(21), 4619.
160 P. L. W. Tregenna-Piggott, L. W. Philip, H. Weihe and A.-L. Barra, *Inorg. Chem*., 2003, **42**(25), 8504.
161 M. Ito, S. Onaka, H. Ebisu, M. Arakawa, Y. Yamada and T. Yoshida, *Inorg. Chim. Acta*, 2003, **353**, 51.
162 Y. M. Hase, Y. Ito and Y. Tajima, *J. Phys. Chem. B*, 2005, **109**(40), 18942.
163 V. I. Volkov, K. K. Pukhov, S. H. Choh, I.-W. Park and E. V. Velkov, *Appl. Magn. Reson*., 2003, **24**(2), 177.
164 P. S. Gahlot, V. P. Seth, A. Agarwal, N. Kishore, S. K. Gupta and M. Arora, *J. Phys. Chem. Solids*, 2005, **66**(5), 766.
165 A. Krupska, *Mol. Phys. Rep*., 2005, **41**, 104.
166 T. Chivers, D. J. Eisler, C. Fedorchuk, G. Schatte, H. M. Tuononen and R. T. Boere, *Chem. Commun*., 2005, **31**, 3930.
167 A. K. Singh and R. Mukherjee, *Dalton Trans*., 2005, **17**, 2886.
168 F. Paul, L. Toupet, J.-Y. Thepot, K. Costuas, J.-F. Halet and C. Lapinte, *Organometallics*, 2005, **24**(22), 5464.
169 G. L. Hug, D. M. Camioni and I. Carmichael, *J. Phys. Chem. A*, 2004, **108**(31), 6599.
170 I. Streeter, A. J. Wain, J. Davis and R. G. Compton, *J. Phys. Chem. B*, 2005, **109**(39), 18500.